CHALMERS
UNIVERSITY OF TECHNOLOGY

Analysis of the Propulsion System of an Electric Aircraft

Master's thesis in Sustainable Electric Power Engineering and Electromobility

Smita Smita, Chandrima Kollara Pradeep

DEPARTMENT OF ELECTRICAL ENGINEERING

CHALMERS UNIVERSITY OF TECHNOLOGY
Gothenburg, Sweden 2023
www.chalmers.se

Master's thesis 2023

Analysis of the Propulsion System of an Electric Aircraft

SMITA SMITA
CHANDRIMA KOLLARA PRADEEP

CHALMERS
UNIVERSITY OF TECHNOLOGY

Department of Electrical Engineering
Division of Electric Power Engineering
Chalmers University of Technology
Gothenburg, Sweden 2023

Analysis of the Propulsion System of an Electric Aircraft
SMITA SMITA
CHANDRIMA KOLLARA PRADEEP

Supervisors: Giacomo Mingardo, Johan Hellsing, Heart Aerospace AB
Examiner: Stefan Lundberg, Department of Electrical Engineering

Master's Thesis 2023
Department of Electrical Engineering
Division of Electric Power Engineering
Chalmers University of Technology
SE-412 96 Gothenburg
Telephone +46 31 772 1000

Cover: Heart Aerospace ES-30.

Typeset in LaTeX
Printed by Chalmers Reproservice
Gothenburg, Sweden 2023

Abstract

This thesis focuses on the design and development of control laws, specially crafted for the propulsion system of the ES-30 aircraft, a creation of Heart Aerospace AB. The ES-30 distinguishes itself as a hybrid electric aircraft, designed for regional travel and outfitted to accommodate 30 passengers. This study unfolds the intricate relationship between the propulsion system and the electrical counterparts, outlining the control laws and the effective functioning of this aircraft.

The control function is a network that feeds on the thrust request and air data as its inputs and provides RPM and pitch angle as outputs. This strategic combination is designed to deliver the requested thrust while concurrently maximizing the efficiency of the propulsion system. This idea is taken one step further by accounting for electrical losses that pervade through the propulsion system. These losses are primarily attributed to motor and inverter losses, which vary across different operational phases and time duration. They are integrated into the system-wide considerations to determine the final propeller pitch and motor RPM. Such a holistic approach guarantees a comprehensive understanding of the system's functioning and the implementation of the most efficient control laws.

From our analysis, it has been determined that the optimal RPM - pitch combinations for the Take off, Climb and Cruise flight phases are 1750 rpm and 20.3°, 1650 rpm and 29.15°, 1350 rpm and 31.7°respectively. These combinations offer optimal efficiency during the associated flight phases, a conclusion derived from thorough analysis. The average efficiency of the flight across the Take off, climb and cruise phases for when optimizing for the the propeller efficiency alone was noted to be 82.43 % and compared to 82.49 % when optimizing for the entire propulsion system efficiency. It was also observed that the propeller's and the entire propulsion system's optimum operating point is at the same RPM for flight phases with higher thrust demand - Take Off and Climb, while they are different for the phases with lower thrust demand, Cruise. Since the aircraft is in Cruise for the longest time, it makes a difference in the performance of the aircraft.

Keywords: Electrical aircraft, thrust, efficiency, thermal, motor, pitch, RPM, algorithm, comparison.

Acknowledgements

We wish to express our heartfelt gratitude and sincere thanks to everyone who has supported us during the undertaking of this thesis, a journey that has been both challenging and rewarding.

First and foremost, we would like to extend our deepest appreciation to our thesis advisor, Stefan Lundberg whose invaluable guidance, patience, and expertise have significantly shaped the outcome of this work. His unwavering belief in our abilities, constant encouragement, and dedication to the highest academic standards have greatly motivated and inspired us. We are indebted to the entire team at Heart Aerospace AB, especially Giacomo Mingardo and Johan Hellsing, who provided us with the necessary resources, data, and crucial insights into the ES-30 aircraft that served as the backbone of our study. Their collaboration and willingness to engage with us enriched the quality of this research. We are also obliged to Hartzell Propellers, who provided us with the adequate non-proprietary data for the propeller performance to be used in this publication.

Additionally, we express our gratitude to our peers and fellow researchers at Chalmers University of Technology, whose stimulating discussions and constructive critiques have brought more depth to our understanding and clarity to our thoughts. Our camaraderie will forever be one of the most cherished aspects of this journey.

Lastly, to our family and friends who have been a constant source of encouragement, laughter, and perspective, we say thank you. Your support has been invaluable. This thesis is the culmination of many people's efforts, and each of you has been an integral part of this journey. We are truly grateful for your help and encouragement, without which this work would not have been possible.

Smita Smita and Chandrima Kollara Pradeep, Gothenburg, June 2023

List of Acronyms

Below is the list of acronyms that have been used throughout this thesis listed in alphabetical order:

AC	Alternating Current
BMS	Battery Management Systems
CFD	Computational Fluid Dynamics
DC	Direct Current
EPACS	Electrical Propulsion Actuation and Control System
EPS	Electrical Propulsion System
EPU	Electrical Propulsion Unit
FEA	Finite Element Analysis
PMSM	Permanent Magnet Synchronous Machine
RPM	Revolutions Per Minute
SOC	State of Charge
SOH	State of Health

Nomenclature

Below is the nomenclature of indices, sets, parameters, and variables that have been used throughout this thesis.

Parameters

M_{tip}	Mach Tip
V_0	Aircraft Speed
n	speed of the propeller
D	Diameter of the propeller
γ	Adiabatic Index
θ	Air Temperature
λ	Conductive Heat Transfer Coefficient
h	Convective Heat Transfer Coefficient
α	Radiative Heat Transfer Coefficient
k	Contact Heat Transfer Coefficient
R_*	Air Constant
ρ	Air Density
T	Thrust
Q	Torque
P	Absorbed Power
C_T	Thrust Coefficient
β	Blade Angle
η	Efficiency
C_P	Power Coefficient
J	Advanced Ratio

Variables

θ	Electrical Angle
ω_e	Electrical Rotor Speed
ψ_f	Flux linkage in rotor excitation
ψ_d	Flux linkage in d-axis
ψ_q	Flux linkage in q-axis
L_d	Inductance in d-axis
L_q	Inductance in q-axis
i_d	Current in d-axis
i_q	Current in q-axis
u_d	Voltage in d-axis
u_q	Voltage in q-axis
R_s	Stator Phase Resistance
$T_{coolant}$	Coolant Temperature j
$T_{winding}$	Motor Temperature
Ts	Sampling Time
R_{th}	Thermal Resistance
C_{th}	Thermal Capacitance
$P_{Cu,loss}$	Copper Loss for the entire propulsion unit

Contents

List of Figures

1

Introduction

1.1 Background

In our rapidly evolving world, with increasing technological advancements, worsening climate crisis, and growing environmental consciousness, is challenging the emissions from different modes of transport. In particular the booming industry of air travel, is quickly becoming the need of the hour. While the Kyoto Protocol clearly specifies the obligations of individual nations to cut down greenhouse gas emissions, the international transport was not included. The International Civil Aviation Organisation (ICAO) was made responsible for dealing with air emissions [1]. The ICAO hence laid down regulations to control CO_2 emissions of civil aircraft [2] and certification standards for noise and NO_x levels in commercial flights for the 2020s [3]. The pioneers in the aerospace and aircraft industry like NASA, and Boeing have developed aircraft technologies with different electric propulsion configurations for regional jets and larger aircraft to address this challenge [4]. Airbus and many start-ups like Volocopter have even launched the concept of electric Vertical Take Off and Landing (eVTOL) for their aircraft [5].

These aircraft represent a significant shift from traditional combustion engine models, potentially promising a cleaner and more efficient future of aviation. Aerodynamics has always been a central theme in aviation, with propellers and aero engines being the heart of a propulsion system. By propelling the aircraft forward using thrust generated from the rotation of the blades, propellers play a key role in the flight. In an electric propulsion system, the efficiency of the propellers becomes even more vital due to the limitations of battery technology.

In parallel, the electric motor, the "muscle" of an electric aircraft, is also a critical component. Their operating points, such as voltage, current, and rotational speed, are vital to the overall efficiency of the system. These motors differ significantly from traditional combustion engines and thus demand a different set of considerations and strategies for optimization.

The central theme of this thesis is an analysis of the dependence of efficiency on the propellers and the electric motor operating points in such an electric propulsion system. The work aims to uncover new insights into how these systems function and how their efficiency can be maximized. This study will delve into the effects of propeller design and operating conditions on overall system efficiency. The analysis

will shed light on how various operating points impact the system's overall efficiency.

The company in focus in this thesis is Heart Aerospace AB, a Swedish start up formed with the intention to electrify regional air travel and thus be a key player in tackling the issues mentioned above. The ES-30 aircraft is a hybrid electric aircraft with battery systems as the primary energy source and reserve turbo generators as the secondary energy source, and it is propelled by 4 electric motors. The 30 seat aircraft has a typical range of 200 km (all-electric), 400 km (electric+hybrid) and 800 km (electric+hybrid with 25 passengers).

This thesis embarks on a comprehensive exploration to ascertain the optimal efficiency of an aircraft propeller during each phase of flight and subsequently provides appropriate instructions for revolutions per minute (RPM) and blade pitch to the respective controllers. It aims to uncover the intricate dynamics governing the aircraft's propeller performance, and the ripple effects this performance has on the overall flight operation. This is achieved by systematically commanding the corresponding RPM and blade pitch, parameters that have a profound impact on propeller performance, and transmitting these values to their respective controllers. This process forms the crux of the work and is designed to yield insights that could potentially lead to significant improvements in aircraft efficiency.

It is recognized that the propeller doesn't operate in isolation. Instead, it's an integral component of an interconnected system, and its performance is inherently tied to the efficiency and losses within the electrical system. Therefore, it is essential to investigate how changes in the electrical system's efficiency and losses reverberate through to the propeller's efficiency and operating point.

This dual-pronged approach of investigating the propeller's efficiency in conjunction with the electrical system's performance allows to capture a more accurate and nuanced understanding of the aircraft's propulsion system. It gives the capability to make more informed recommendations on optimizing propeller performance, ultimately enhancing the overall efficiency and performance of the aircraft.

1.2 Aim

The central objective is to determine the electric propulsion unit's most efficient operating point - a crucial aspect affecting an aircraft's fuel efficiency, emissions, and operational costs.

In tandem to this, the correlation between the electrical system's efficiency and losses, and their cumulative effect on the propeller's efficiency and operating point should be examined.

1.3 Scope and Limitations

This thesis extends to all prototypes of short-haul, propeller-based electrical aircraft. It employs a theoretical model of the electrical propulsion unit, allowing for a high degree of adaptability, as all experimental variables and their ranges can be adjusted based on specific requirements.

A notable boundary of this study is its reliance on performance data for the propellers provided by Hartzell. This data, which has undergone comprehensive calculation, testing, and verification by the supplier, constitutes the foundation for the propeller constants and experimental value ranges used in the research. While there is no direct calculation, modification, or justification provided in the selection of these constants, they are derived from reasonable consideration of the given propeller data.

The findings of this study are theoretical in nature and have been modeled using MATLAB software. This approach bypasses potential inaccuracies that could arise from factors such as physical properties, equipment resistance, and human intervention. While this method does ensure a high degree of accuracy in the results, it's important to remember that real-world application may introduce variables not accounted for in a theoretical model.

Lastly, the study treats the battery management systems, the power electronic converters, and the aircraft data systems as 'black boxes'. This means that while their respective outputs, losses, and functions have been considered during the course of the experiments, the intricate details of their internal workings are not investigated within the scope of this research. The use of the 'black box' approach, while practical for the objectives of this study, may oversimplify the complexity and interplay of these systems in actual operational settings.

In conclusion, while this thesis presents a comprehensive theoretical exploration into the performance of electrical propulsion units in short-haul, propeller-based aircraft, it is crucial to understand its limitations. Future work might focus on enhancing the level of detail in modelling these 'black box' systems and performing empirical testing to validate the theoretical models developed here.

2

Theory

2.1 Basics of Aviation

Airplanes with propellers, often referred to as propeller-driven aircraft, rely on a combination of aerodynamics and mechanical propulsion to achieve and maintain flight. The core concepts behind their operation date back to the earliest days of aviation, but modern technological advancements have drastically increased their efficiency and reliability.

The principle of flight for propeller-driven aircraft is based on Bernoulli's principle, which states that an increase in the speed of a fluid occurs simultaneously with a decrease in pressure. In the context of aviation, the fluid is the air that the aircraft moves through. The wings of an aircraft are designed with a special shape, known as an airfoil, which is typically curved on the top and flatter on the bottom. In the case of an un-accelerated and steady flight, there are generally two types of forces at work, one being the body force and the other being the surface force. The body force acts on the body from a distance, which in this instance is weight and gravity, while the surface force acts because of the contact between the airplane and the air, which in this case is lift, thrust, and drag [6]. At its core, the flight of an airplane can be broken down into a balance of four main forces: lift, weight (or gravity), thrust, and drag.

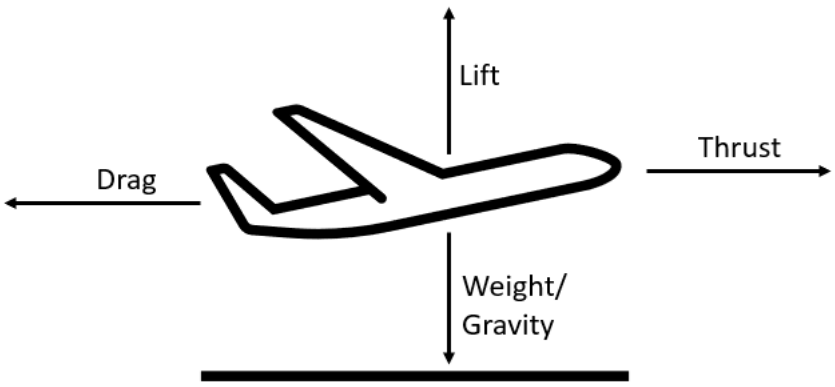

Figure 2.1: Forces acting on an Aircraft

1. **Thrust**: This is the forward force that moves the airplane through the air. It's generated by the plane's propellers. As the propellers spin, they pull or push the aircraft forward. When the thrust exerted becomes greater than the drag effect, the aircraft starts moving. Thus, when the thrust is greater than the drag, the aircraft accelerates and it decelerates when thrust is less than the drag [7].

2. **Drag**: This is the air resistance that the plane encounters as it moves forward. It's a force that opposes the direction of flight. The airplane must produce enough thrust to overcome this drag. There are basically two types of drag that act on the aircraft: Parasite Drag and Induced Drag. The parasite drag is called so because it consistently hinders the flight. The induced drag is created as a result of the lift on the airfoil [7].

3. **Lift**: This is the upward force that allows the plane to rise and stay in the air. Lift is produced by the flow of air over and under the wings. It always acts perpendicular to the aircraft's lateral axis and the relative wind. The wings are designed in a special shape, called an airfoil, which makes air move faster over the top of the wing and slower underneath. According to Bernoulli's principle, faster-moving air has lower pressure, so this creates an upward force on the wing. The lift counteracts the weight and aids a level flight when both these forces are equal. The aircraft accelerates vertically when lift is greater than the weight and decelerates vertically when lift is less than the weight [7].

4. **Weight/Gravity**: This is the downward force that pulls the airplane towards the Earth. It includes the complete weight of the aircraft including the weight of the fuel, cargo, passengers, etc. To stay in the air, the airplane must generate enough lift to counteract its own weight.

2.2 Different Phases of a Flight

The process of flight can be compartmentalized into seven distinct phases, each contributing to the progression of the aviation journey from taxiing to final destination. They delineate the aircraft's movement, providing a systematic narrative that guides the operations at each stage. In Figure 2.2 the seven phases are shown with their corresponding flight altitude. The phases delineate the aircraft's movement, providing a systematic narrative that guides the operations at each stage.

- **Taxi Out Phase**: This initial stage involves the aircraft's movement from its stationary position at the designated gate to the ready position on the runway. Here, the aircraft navigates the airfield under the guidance of ground crew and air traffic control. It prepares to transition from land to the airborne journey.

- **Take-Off Phase**: This critical stage involves the aircraft's acceleration along the runway, the nose lifting skyward as it reaches the required velocity. It

is a period of transition, requiring careful coordination between the aircraft's controls, propeller thrust, and aerodynamic forces at play. Out of all the flight phases, Take off is the relatively shorter but intense phase. The aircraft accelerates from zero speed to its lift off speed to make it airborne [8]. It is required to lift the complete weight of the aircraft from ground to the air here. Since minimum take off distance determines the requisites of a runaway, maximum thrust and acceleration are required to achieve the same at a safe lift off speed [7]. This phase can last anywhere between a couple of seconds to couple of minutes.

- **Climb Phase**: This phase can be considered as a continued maneuver from the take off. It involves the aircraft's further ascend to its cruising altitude. The aircraft must negotiate a delicate balance between altitude gain and speed maintenance, while also adjusting to the changing atmospheric conditions like the air density and sharply dropping temperature and pressure. As the aircraft is already airborne and the air parameters drop significantly, the thrust demand also drops [7].

- **Cruise Phase**: The cruising phase is marked by relative stability. Here, the aircraft glides across the sky at a consistent altitude and speed, covering significant distances as it makes headway toward its destination. This period of the flight is the longest and is characterized by the maintenance of the equilibrium that the aircraft has achieved, balancing forces of lift, gravity, thrust, and drag. Since there is no requirement for vertical or horizontal acceleration here, the thrust is comparatively lower with respect to the take off and climb phases [7].

- **Descent Phase**: This stage sees the aircraft gradually reducing altitude, maneuvering its way downwards through the atmospheric layers towards the landing site. This is a carefully regulated phase, requiring a calculated balance between speed reduction and descent rate.

- **Approach and Landing Phase**: As the aircraft aligns with the runway, this phase marks the end of the aerial journey and the transition to ground movement. The aircraft makes contact with the ground, decelerating until it reaches taxiing speed.

- **Taxi In Phase**: The concluding stage of the journey, this phase sees the aircraft navigating its way along the runway to its designated gate.

This thesis focuses on the Take-Off, Climb, and Cruise phases. These periods of the flight are critical for they dictate the operational efficiency and overall performance of the aircraft.

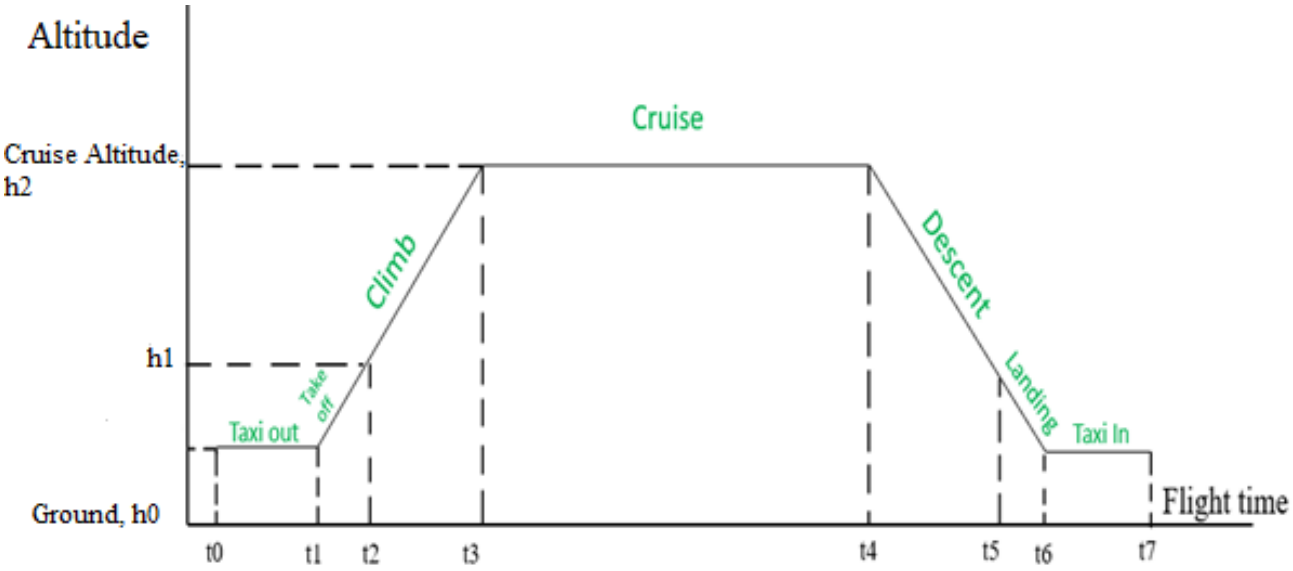

Figure 2.2: Flight Phase Trajectory

2.3 Propulsion System of Electric Aircraft

The forward movement required for generating thrust is provided by the propulsion system, which in a propeller-driven aircraft, includes the electric machine and the propellers. An electric aircraft's propulsion system is comparable to that of conventional automobiles but with the complexity of electrification. It includes a mechanical system that moves or propels the vehicle forward and a power source that provides the required energy. There are various available power sources ranging from conventional aviation fuels to the new emerging fuel cell technology. Based on the level of hybridization of the energy sources used in the aircraft, the electric propulsion architecture can be classified as all-electric, turbo-electric and hybrid electric propulsion [9].

2.3.1 Turbo-Electric

Here, the electric generator that produces the electrical energy is driven by one or more gas turbines. The energy generated by the gas turbine is completely used by the generator as both are directly connected, as can be seen in Figure 2.3 where the architecture of the Turbo-Electric propulsion system is shown. There is no energy storage device in this architecture [9]. Generally a single gas turbine is used in such configurations as it is more efficient than a smaller turbine. Its standard architecture can be described using the Figure 2.3; with application specific variations like added power electronics components, that aid in reducing various conduction and conversion losses, or elimination of the gearbox [10].

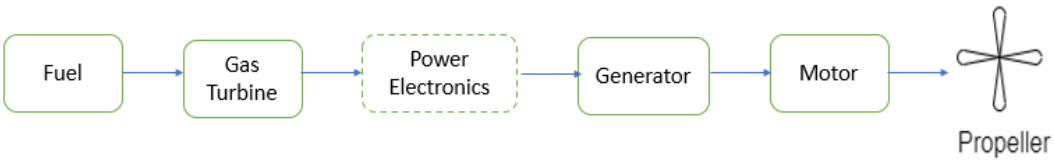

Figure 2.3: Turbo-Electric Architecture

2.3.2 All-Electric

It has a battery source directly connected to the power electronic converter that converts the DC voltage from the battery to an AC voltage that powers the electric motor, which drives the propeller. In Figure 2.4 the architecture of the All-Electric propulsion system is shown. As the battery energy is the only source of energy, this type of aircraft needs to be charged completely before the flight and will be mostly ideal only for short haul flights [9].

This architecture is the simplest among all with a high efficiency energy conversion system and the only architecture that can achieve net zero emissions during the operation [11]. However, the weight of the battery is a challenge here specifically for long haul flights [10].

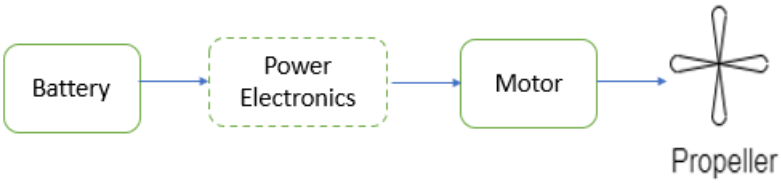

Figure 2.4: All-Electric Architecture

2.3.3 Hybrid Electric

This architecture is the interesting one for this work as the ES-30 aircraft is a hybrid electric aircraft. Like a conventional hybrid automotive, the hybrid aircraft also has many advantages such as increased range, low emissions, minimal fuel burn etc. The required thrust power is delivered by battery alone, turbine alone or both. The energy sources balance during the flight to obtain the optimum operation. There are two main types of configurations in this case [9], the series hybrid and the parallel hybrid, and they are explained in the following section:

2.3.3.1 Series Hybrid Electric Architecture

In this configuration, the propellers are driven only by the motor. The energy from the generator, which is in turn created by the turbine, runs the motor and/or is

used to charge the batteries [9]. In Figure 2.5 the architecture of the series hybrid propulsion system is shown. This is the configuration implemented specifically in the ES-30.

There are various advantages in this case as the generator is not directly connected to the propellers. The energy converted by the generator can be used to recharge the battery during low thrust demand phases like Cruise. The turbine can constantly operates at its best power and speed configurations. While this is optimal for low speed operations and makes the propulsion control easy, it requires heavier electrical components, thus increasing the weight of the whole system [12].

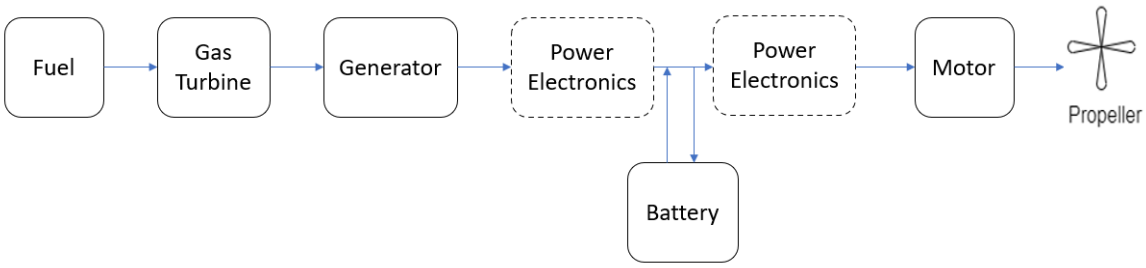

Figure 2.5: Series Hybrid Architecture

2.3.3.2 Parallel Hybrid Electric Architecture

In the parallel hybrid electric architecture, shown in Figure 2.6, the two power sources, gas turbine and electric motor are mechanically coupled in parallel and drives the propeller either simultaneously or individually. Compared to the series hybrid architecture, the electric generator is absent here. Hence the smaller sized electrical components can be used as both the sources can provide the required power.

One drawback is that the gas turbine can not always be operated at its best operating point. Furthermore, use of a gearbox, needed to adapt the speed of the gas turbine to the speed of the propeller, adds more weight to the whole system. The mechanical coupling establishes the need for an intricate propulsion control system [12].

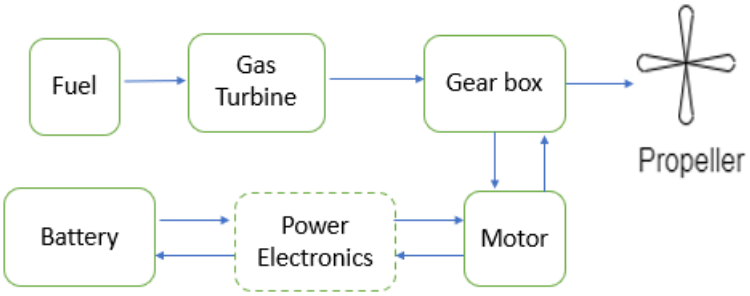

Figure 2.6: Parallel Hybrid Architecture

2.4 System Architecture

2.4.1 Propeller: Theory and Control

The aircraft propeller can be considered as a rotating wing of the aircraft which converts the rotational or mechanical energy, from a power source which is an electric motor in this case, to thrust that propels the aircraft. The basic mechanism of thrust generation is to use the energy to displace and accelerate a certain amount of air according to Newton's third law of motion. A propeller usually consists of two or more blades which are attached to a central hub [16].

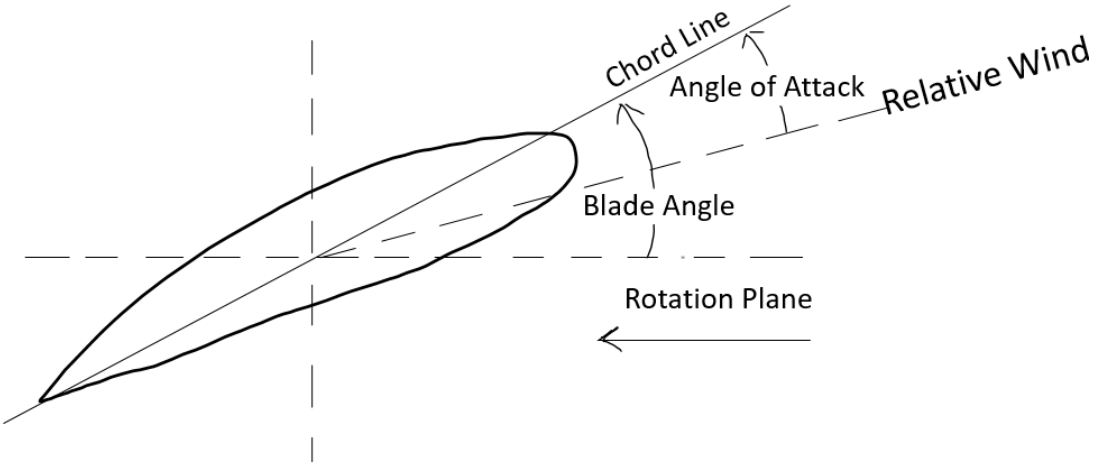

Figure 2.7: Propeller Anatomy

A representation of a propeller cross-section is shown in the Figure 2.7. This can be compared to the cross-section of an aircraft wing. An imaginary line drawn along the face of the propeller blade is the chord line. Blade angle (hereafter referred to as propeller pitch) is the angle measured at a certain point along the blade, between the chord line and plane of rotation. The wind strikes the blade at a certain angle called the angle of attack, which can be regulated with the pitch angle [16]. The propeller performance is usually designed and analyzed using the following dimen-

sionless parameters:

Mach Tip, M_{tip}: It is the ratio between the propeller tip speed and the speed of air.

$$M_{tip} = \frac{\sqrt{V_0^2 + n\frac{D}{2}^2}}{\sqrt{\gamma R_* \theta}} \tag{2.1}$$

Advanced Ratio, J: It indicates how far the propeller advances per revolution in terms of its diameter and is given by

$$J = \frac{V_0}{nD} \tag{2.2}$$

Thrust Coefficient:

$$C_T = \frac{T}{\rho n^2 D^4} \tag{2.3}$$

Torque Coefficient:

$$C_Q = \frac{Q}{\rho n^2 D^5} \tag{2.4}$$

Power Coefficient:

$$C_P = \frac{P}{\rho n^3 D^5} \tag{2.5}$$

where V_0 is the aircraft speed, n is the speed of the propeller, D is the diameter of the propeller, γ is the Adiabatic index, R_* is the air constant, θ is the air temperature, ρ is the density of the air, T is the thrust, Q is the torque and P is the absorbed power.

One of the main challenges faced by the high altitude propellers is the low air density. The air density dramatically decreases the higher you travel and at the heights of 20 and 25 k feet the density value fall in the range of 30 to 40 percent, roughly 41.6 and 37.6 kPa respectively, of the sea level value, which is 101.3 kPa. This results in a very low working Reynolds number value, which results in major changes within the airfoil performance [18]. This directly affects, and deteriorates the aerodynamic performance which in turn decreases the propeller efficiency.

Another big challenge with high altitude propeller design is the working combination of the electrical motors and the propellers on ground or low altitude levels. When the propellers are used at a low altitude, the higher values of air density limit the rotational speeds of the propellers due to a restriction on the maximum torque, which results in low values of thrust and shaft power as well [18].

2.4.2 Variable pitch propellers

Addressing the challenges encountered in electrical propulsion systems, one viable solution lies in the utilization of a variable pitch propeller. The blade pitch angle is fundamental to airfoil development and interaction, as changes in pitch directly impact the angle of attack, as well as lift and drag components, rotational speed, shaft power, and thrust.

Decreasing the pitch angle results in a corresponding decrease in the effective angle of attack, lift, and drag components. Conversely, this reduction leads to an increase in rotational speed, thrust, and shaft power. These changes can enhance the harmony between the electrical propulsion unit and the rotating/mechanical units, leading to a more efficient operation [18].

Variable pitch propellers are already widely incorporated in various aircraft designs, especially those operating at high altitudes [18]. The ES-30 employs a variable pitch propeller with the primary aim of achieving maximum efficiency under a given set of air parameters. These parameters are dynamically fed into the objective function from the connected cockpit and control units. The pitch angle is determined based on achieving the maximum efficiency for the propellers during operation.

The ES-30 aircraft, for instance, utilizes a variable pitch propeller consisting of five blades. This setup is indicative of the growing trend of leveraging variable pitch propellers to optimize performance and efficiency in electric aircraft propulsion systems.

2.4.3 Permanent Magnet Synchronous Machine (PMSM)

The Permanent Magnet Synchronous Machine (PMSM) stands as a distinct classification within the family of alternating current (AC) synchronous machines. One could perceive this machinery as an innovative blend of a brush-less DC motor, boasting a congruent permanent magnet rotor and stator winding, and an Induction motor, sharing a similar sinusoidal airgap flux density pattern. The uniquely designed rotor within the PMSM gains its magnetization from inherently incorporated permanent magnets.

The creation of PMSM can follow two distinctive paths, each primarily differentiated by the spatial placement of the permanent magnets concerning the rotor [13]. Regardless of the construction approach, the fundamental operating principle remains the same for both variants.

The working of a PMSM can be described as follows: An external alternating power supply energizes the three-phase stator winding, thereby generating a rotating magnetic field within the airgap. This magnetic field then becomes 'locked' by the rotor poles, ultimately resulting in the production of torque, which sets the motor shaft into motion [25].

PMSM machines are more commonly used within the electrical vehicle sector due to the following reasons [13] -

1. High power factor, high efficiency and improved overload capacity.
2. Large torque inertia ratio, larger torque output at lower speeds result in better starting acceleration profile.
3. No rotor copper loss, reducing the motor losses and make it a more sustainable option, since there is no secondary magnetic field excitation.
4. High power density and smaller moment of inertia which along with increasing the magnetic flux density, make the motor more compact and thus a better choice for space restrictive applications.

The mechanics and unique attributes of the PMSM can be better comprehended by diving into a more comprehensive exploration of its key components, as will be elaborated in the following subsections [13].

2.4.3.1 Stator

Integral to the operation of an electric motor, the stator serves as a stationary counterpart to the motor's rotor. This immobile component creates an envelope around the rotor, functioning as a pivotal element in the motor's operation by generating a dynamic, rotating magnetic field. The stator's construction typically includes a core, primarily composed of laminated iron sheets that are purposefully structured to reduce energy losses that can occur due to eddy currents. The iron sheets improve the magnetic permeability of the stator, allowing for an efficient pathway for the magnetic flux, which is essential for the generation of the magnetic field [19].

In addition to the core, the stator incorporates a series of copper wire windings or coils. These coils, painstakingly arranged in intricate patterns, become the avenue for electric current flow, thereby creating the intended electromagnetic fields. This specific arrangement is not arbitrary but is derived from carefully calculated design choices to optimize motor performance [19]. When an electric current is introduced, it courses through these copper winding, instigating the creation of electromagnetic fields. As these fields interact with the magnetic fields produced by the rotor, a force is generated. This interaction induces a rotational motion in the motor shaft, which is essentially the conversion of electrical energy into mechanical energy.

In essence, the stator's role is central to the motor's function, laying the foundation for the electric motor's fundamental operational principle: to transform electrical energy into usable mechanical energy [19].

2.4.3.2 Airgap

The airgap, defined as the distance between the rotor and stator, plays a pivotal role in a motor's performance and efficiency. It represents the non-conductive region through which this magnetic flux must pass and therefore, its size directly affects the magnetic field's efficiency in inducing a torque on the rotor.

A reduced airgap leads to a more potent magnetic field interaction between the stator and rotor. This results in a higher torque. However, the challenge with a smaller airgap is primarily mechanical: ensuring that the rotor doesn't come into contact with the stator, especially during mechanical resonances or vibrations. Additionally, the intensified magnetic interactions produce increased heat, implying potential thermal management challenges.
On the other hand, an enlarged airgap can be a hindrance. It effectively weakens the magnetic field's strength, potentially reducing the torque and overall efficiency of the motor. This emphasizes the importance of precision in airgap design, which seeks to optimize the balance between power, efficiency, and stability in electric motor design [20].

2.4.3.3 Rotor

Acting as the dynamic portion of the motor, the rotor's primary function is to generate the output motion, more specifically, the torque that turns the mechanical components attached to it. These critical functions underscore its essentiality in the operation of an electric motor [21].

This indispensable component generally takes the form of a cylindrical core, constructed from laminated layers of iron or steel. The utilization of these materials in a laminated structure effectively reduces losses due to eddy currents, a phenomenon where swirling currents produced within the conductor lead to energy dissipation as heat [21]. The core is then affixed to a shaft, providing a connection to the mechanical systems that the motor propels.

Integral to the rotor operation in a PMSM are permanent magnets, rather than conductive elements like coils or bars found in other motors. These magnets are positioned in a pre-defined pattern, engineered to maintain a consistent magnetic field [21]. The exciting event occurs when a three-phase electric current is passed through the stator windings. In response, a rotating magnetic field is generated. This field interacts with the constant magnetic field produced by the rotor's permanent magnets. As these fields interact, a synchronous rotational force is invoked upon the rotor [21]. This is the key interaction that drives the operation of a PMSM, illustrating the essential role the rotor plays in the energy conversion process.

2.4.3.4 Mathematical modelling of a PMSM in D-Q coordinate system

Mathematically a PMSM can be explained in a two phase, dq synchronous rotational coordinate system [14]. Some assumptions to make this equivalence possible are taken, which are the following:

1. No consideration of the magnetic saturation and the effects of magnetic hysteresis.
2. Ignoring the eddy currents and their subsequent losses.
3. Assuming the rotor has no damper winding.

4. Assuming a sinusoidal distribution for the magnetic flux in the motor air gap, with no high values of harmonics.
5. Assuming total inter-linkage of the PMSM flux.

In this two axis coordinate system, the d-axis is aligned with the magnetic field axis. Consequently the q-axis as the electrical axis which is perpendicular, or at a 90° anticlockwise angle, to the d-axis. The angle between the magnetic field, or d-axis, and the stator winding is then given by θ, which rotates with the rotor electrical speed ω_e. This gives a general D-Q flux linkage equation for the PMSM model in [14] as given,

$$\begin{bmatrix} \psi_d \\ \psi_q \end{bmatrix} = \begin{bmatrix} L_d & 0 \\ 0 & L_q \end{bmatrix} \begin{bmatrix} i_d \\ i_q \end{bmatrix} + \begin{bmatrix} \psi_f \\ 0 \end{bmatrix} \tag{2.6}$$

where L refers to the inductance, for the d and q axis as denoted by the subscript, ψ_f gives the flux linkage of rotor excitation flux through stator winding and i is the d and q axis current. Similarly ψ_d and ψ_q for flux linkage related to both d and q axes respectively. Using this relation, the voltage can be expressed as:

$$u_d = R_s i_d + L_d \frac{d}{dt} i_d - \omega_e L_q i_q \tag{2.7}$$

$$u_q = R_s i_q + L_q \frac{d}{dt} i_q - \omega_e L_d i_d + \omega_e \psi_f \tag{2.8}$$

where R_s is the stator phase resistance, u_d and u_q are d and q stator voltages respectively and ω_e is the electrical angular speed of the rotor.

For the dq-model, the torque can be calculated as

$$Q = \frac{3}{2} * p * (\psi_f i_q + (i_d i_q) * (L_d - L_q))) \tag{2.9}$$

where p is the number of pole pairs.

2.4.4 Lumped parameter thermal modelling

A thermal model of an electrical machine can be based on the electrically analogous heat transfer flow model, between the various parts of the working machine, in this case, a PMSM. In order to make optimal decisions regarding the power train component selections, accurate economy and life target measurements and mapping the performance of the entire power train, the influence of heat losses on the various parts is an important consideration.

Electric vehicles in particular have a focus on the development of thermal models with the aim of optimising the power and torque utilisation at the lowest possible thermal losses and damage [15]. The most popular models used in the industries are

CFD and FEA, with their ability to locate thermal hot-spots and suggest possible design changes, although they are quite detailed and thus require higher computation efforts to build especially for a system level analysis.

Another model, used in this analysis, is called a lumped parameter thermal model, where a grey box, or lumped modelling technique is utilised. It is a combination of a data driven and physics based model that represents the thermal inertia of respective components as their equivalent thermal resistance and capacitance to make the state flow simpler for analysis. The developed energy equations are then solved inside the state space and component temperatures are calculated over the response time. This can be used to develop loss models for the different components, in particular the core and copper loss models for the PMSM, that can be further used to give an optimised efficiency map for the same power train.

Such a model is approximately 100 times less computationally expensive, and has an estimated temperature difference of around 2% when compared to the traditional detailed analysis models [15]. Thus, such a model works very well for a system level study of a power train model.

2.4.5 Parameters of the lumped parameter network model

There are two main types of variables in a lumped parameter model, thermal resistance and thermal conductivity. Together with an applied power and the heat flow path, they make up the most basic thermal network model. Thermal resistance, quite similar to its electrical namesake, is a material's ability to resist the heat flowing through its body. It is inversely related to the thermal conductivity of the material. The unit of thermal resistance is K/W, where K is the absolute temperature unit kelvin and W is the SI unit of power, watt.

There are mainly four types of thermal resistances: conductive thermal resistance, convective thermal resistance, radiating thermal resistance, and contact thermal resistance.

The conductive thermal resistance is responsible for the heat transfer within the same material. In a PMSM, it exists in both the solid parts and the motionless gaseous makeup of the airgap. It can be calculated as,

$$R = 1/(\lambda A);$$

where λ is the conductive heat transfer coefficient and A is the area of the conducting surface. The value of λ depends on the temperature of the material, the higher the value the more heat is conducted by the material.

The convective heat transfer resistance depends on viscosity of the coolant, the thermal conductivity, specific heat capacity and the flow velocity of the medium. It can be calculated as,

$$R = 1/(hA);$$

where h is the convective heat transfer coefficient and is determined according to

the Nusselt number, and A is the area of the conducting surface.

The thermal radiation resistance is analogous to the conductive resistance and depends strongly on the temperature of emitting and absorbing surfaces. It can be calculated as,

$$R = 1 /(\alpha A);$$

where α is the radiative heat transfer coefficient and A is the area of the surface emitting or absorbing, depending on the application of the formula.

The thermal contact resistance, stems from the improper contact between two surfaces and is calculated as,

$$R = 1/(kA);$$

where k is the contact heat transfer coefficient due to improper contact and A is the area of surface in contact. It is the most difficult to model and predict since it depends on the manufacturing process and varies for every surface.

In a multiple parameter model, thermal resistance is additive in series. In a given material, it can usually be modeled for junction-to-junction, junction-to-case, junction-to-ambient, junction-to-top of the material or package, etc. All devices come with their thermal information as it plays a huge role in deciding the inputs and insulation material for the given material.

Thermal capacitance, also known as heat capacity, is a fundamental property of any material, signifying its ability to store thermal energy. This property plays an instrumental role in defining the transient characteristics of a machine, aiding in the simulation of its behavior under different thermal conditions.

In a lumped parameter network model, the number of thermal capacitance corresponds to the number of nodes considered when mapping out a heat flow circuit. Each thermal capacitor signifies the heat capacity of a specific part of the machine, making it a crucial component in the thermal modeling of the system. The value of thermal capacitance depends on various parameters: the thermal capacity, the volume and density of the material, and the specific heat capacity of the material. It's expressed in units of Joules per Kelvin (J/K), where Joules (J) represent energy and Kelvin (K) signifies absolute temperature.

The thermal capacitance of a material can be determined in two primary ways:

1. through graphical analysis and by calculation using a specific equation. For the graphical method, a graph between energy and temperature is plotted, and the slope of the curve near the origin is analyzed to derive the value of thermal capacitance.
2. the equation method employs the formula $C = V\rho Cs$. Here, 'V' is the volume of the material being modeled, 'ρ' is the material's density, and 'Cs' refers to the specific heat capacity of the material.

2.4.6 Power Electronic Components

The role of power inverters in electrical aircraft is of paramount importance, acting as pivotal connectors between the energy storage systems and the various electrical systems within the aircraft. They are tasked with the conversion of direct current (DC), supplied by energy storage units like batteries or fuel cells, into alternating current (AC). This AC power is crucial for powering a diverse range of electrical loads and systems that make up the aircraft [23].

One of the primary responsibilities of power inverters in electrical aircraft is supplying AC power to the electric propulsion system. This system is composed largely of electric motors, which are pivotal in providing the thrust required for aircraft propulsion. Most of these electric motors necessitate AC power for their operation. As such, the power inverters serve as an indispensable link, transmuting the DC power sourced from the energy storage system into the requisite AC power. This conversion empowers the electric motors to propel the aircraft, thus fulfilling their primary role [23].

Beyond the propulsion system, power inverters also play a significant role in other aspects of aircraft functionality. They are essential for providing AC power to various other electrical loads and systems in the aircraft. This range encompasses a broad spectrum, including avionics, cabin lighting, environmental control systems, and cabin equipment, to name a few [23]. The majority of these systems are designed to operate optimally on AC power. Thus, the role of power inverters in ensuring the smooth operation of these systems is crucial. By facilitating the conversion of DC power to AC, they enable the seamless operation of a myriad of electrical devices and systems on the aircraft. This contributes substantially to the overall performance and functionality of the electrical aircraft.

Moreover, the sophisticated technology behind modern power inverters allows for efficient power conversion, while also ensuring the quality of the output AC power matches the requirements of the various onboard systems. Power inverters often include features such as voltage and frequency control, short-circuit protection, and overload protection. These features not only ensure reliable operation of the aircraft's electrical systems but also contribute to the safety of the aircraft and its passengers [23].

2.4.7 Battery Management Systems

Within the ecosystem of an electrical aircraft, the Battery Management System (BMS) emerges as a crucial player in guaranteeing the energy storage system's safe and efficient functionality. The BMS serves as the central nervous system for the aircraft's battery, continually monitoring its performance and maintaining optimal operating parameters such as State of Charge (SOC), State of Health (SOH), and temperature. The BMS embodies the concept of intelligent control, managing a multitude of vital functions like cell balancing, voltage and current monitoring, thermal management, and fault detection [24].

Cell balancing emerges as one of the key duties of the BMS. This process ensures that each individual battery cell charges and discharges uniformly, which is of utmost importance in promoting the overall performance of the battery and prolonging its lifespan. The BMS maintains a continuous vigil on the voltage and current of each cell, ensuring balanced operation and safeguarding against potentially damaging disparities among the cells [24].

Additionally, the BMS doubles as a data center, providing essential data points like SOC and SOH. These indicators allow for accurate estimations of the battery's available energy and the overall health status of the battery. This information is integral to maximizing the battery's utilization and facilitating preemptive maintenance, which ultimately enhances the longevity and reliability of the energy storage system.

Thermal management is another critical role shouldered by the BMS. It keeps a constant check on the battery cells' temperature and governs the associated cooling or heating mechanisms to maintain optimal operating conditions. By preventing the battery from overheating or becoming excessively cold, the BMS ensures the safe and efficient performance of the energy storage system.

Moreover, the BMS is armed with sophisticated fault detection capabilities. It actively monitors the battery for any abnormal behavior, such as over voltage, under voltage, over current, or short circuits. When any irregularity is detected, the BMS can activate alarms or initiate corrective measures to mitigate potential risks. This vigilant surveillance system protects not only the battery but also the aircraft as a whole, thereby ensuring the safety of the passengers and the integrity of the flight [24].

3

Case Setup

3.1 System Architecture

Figure 3.1 is the representation of the workflow of a single Electrical Propulsion System (EPS) in the aircraft. The ES-30 features four EPS, with identical architecture and components which is discussed in the following sub-sections.

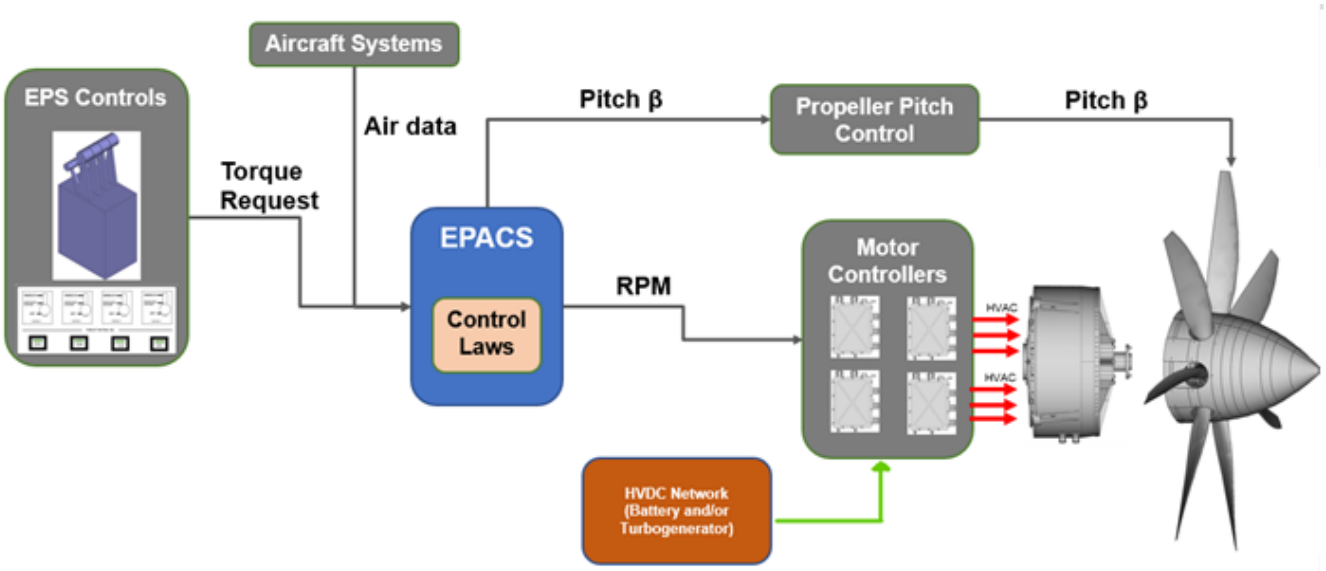

Figure 3.1: EPS Thrust Management Flow

3.1.1 EPS Controls

The Electrical Propulsion System (EPS) control panel in an electric aircraft functions as the crucial communication interface between the pilots and the propulsion system. This interface hosts various control elements, each designed with a specific function that contributes to the overall control of the aircraft's propulsion system. Notably, in the ES-30, the EPS control panel houses different controls: the Start/Stop panel, the Feather panel, and the Thrust Rating Selection panel.

The Start/Stop panel sits within one quadrant of the EPS control panel. This segment includes four individual switches, each corresponding to one of the four EPS units within the aircraft. With these switches, pilots can independently activate or

deactivate each EPS, providing a high level of control and flexibility during different flight phases.

The Feather panel, located in another quadrant, is equipped with four guarded push buttons. These buttons are specifically dedicated to controlling the feathering of each propeller. Feathering refers to the process of adjusting the propeller blades' angle to reduce drag in certain flight conditions, such as engine failure. With these feathering controls, pilots can effectively manage propeller performance, contributing to the aircraft's overall aerodynamic efficiency and safety.

Finally, the Thrust Rating Selection panel is situated in the third quadrant. This panel features four buttons, each designed to select the power or thrust rating for the corresponding EPS. This allows pilots to manually select and control the level of thrust produced by each EPS, catering to various flight conditions and operational requirements.

Overall, the EPS control panel serves as a vital communication and control interface, enabling pilots to manage the electric aircraft's propulsion system effectively.

3.1.2 Aircraft Systems

In an electric aircraft, various systems work in harmony to enable the functionality of the Electrical Propulsion Actuation and Control System (EPACS). One such system provides critical air data parameters as input to the EPACS which include the following:

- Aircraft Speed
- Air Temperature
- Air Density
- Altitude

These standard air data points, delivered to the optimization function as real-time inputs, are updated with each new thrust demand value. These data points and demands, deriving directly from the pilot's controls, are formatted to align with standard air calculation methodologies and match supplier performance graphs. Both the data and the demand come directly from the pilot controls and are fed to the EPACS after manipulating the units to fit the standard air calculation methods and match the supplier performance graphs.

3.1.3 EPACS

EPACS serves as the centerpiece, coordinating the control of the motor and propeller concurrently. It communicates motor speed instructions to the motor controllers and propeller pitch to the propeller controllers. These parameters are strategically optimized to maximize efficiency during each phase of flight.

Although this area remains unexplored in the current work, as per the flight architecture addressed in this thesis, with four motors, the EPACS is also accountable for propeller syncrophasing, ensuring synchronization of the different motors' speeds. Other EPACS functions include managing the thermal aspects of motors, motor controllers, and interacting with the batteries.

3.1.4 Motor Controllers

Each Electrical Propulsion System (EPS) accommodates four motor controllers, one per winding. These controllers manage the motor speed based on inputs from EPACS and house the inverter that transforms the battery's DC power into a 3-phase AC current. This conversion process aligns with the voltage and frequency requirements necessary to achieve the intended motor speed.

3.1.5 Motor

The propulsion of the aircraft is facilitated by a Permanent Magnet Synchronous Motor (PMSM) powered by a 3-phase current flowing through four independent windings, each fed by a distinct motor controller. This configuration also permits the system to operate with partial motor power if a winding or motor controller fails.

3.1.6 Propeller Pitch Control Unit

The Propeller Pitch Control Unit, another crucial component, handles the propeller blade pitch. This hydraulically actuated system activates the propeller hub mechanisms to adjust the propeller blades, achieving the pitch as commanded by the EPACS.

3.1.7 Propeller

The thrust generating unit of the aircraft, the propeller, is a variable pitch propeller with a diameter of 2.9 meters and five blades. There are two propeller sets: one rotating clockwise and the other counterclockwise. The optimal operational configuration is arranged to have the down-going blades positioned in between the nacelles.

3.2 Propeller Performance Optimisation

Hartzell Propeller Inc., a leading company in the propeller manufacturing industry, provided a series of performance maps for a non-proprietary propeller. This propeller is used in the report to show how the propeller performance optimisation is done and the optimisation for the real propeller is performed with the same method and with similar results. These maps, composed of tabular data, outline the Thrust Coefficient (C_T), Blade Angle (β), and Efficiency (η) as functions of Power Coefficient (C_P) and Advance Ratio (J). Each propeller map is characterized by its

discrete helical tip Mach number, resulting in a myriad of data files for each propeller model. This complex data set includes five distinct maps, each correlating with Mach numbers of 0.5, 0.6, 0.7, 0.8, and 0.9. These provide a comprehensive view of propeller performance across a broad spectrum of flight conditions, helping to ensure optimal operation and efficiency.

Figure 3.2 shows an example lookup graph for the propeller performance parameters, efficiency and blade angle. In theses graphs, the Mach numbers are presented on the Z axis, the Power Coefficient (C_P) on the Y axis, and the Advance Ratio (J) on the x axis respectively.

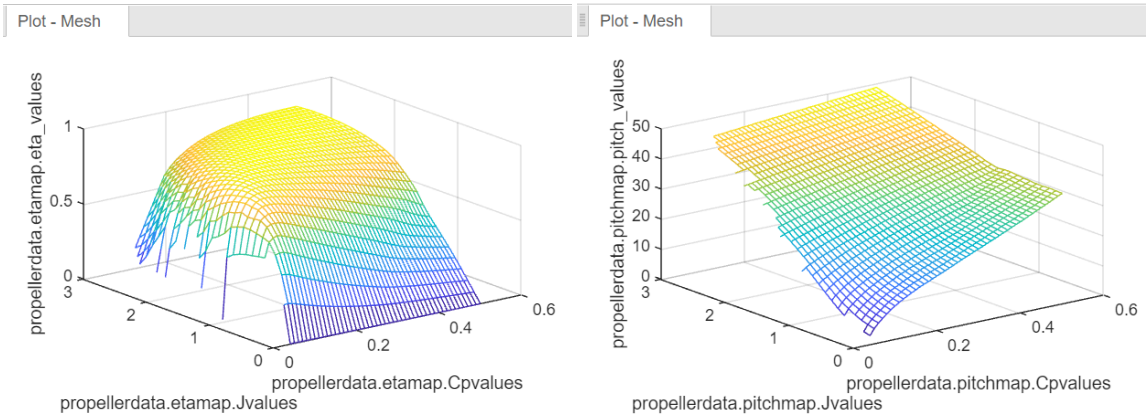

Efficiency Lookup Graph

Blade Angle Lookup Graph

Figure 3.2: Graphical Representation of Lookup Tables for Efficiency and Pitch with flight data on the axes

The block diagram of the control law algorithm is shown in Figure 3.3 and it is implemented as:

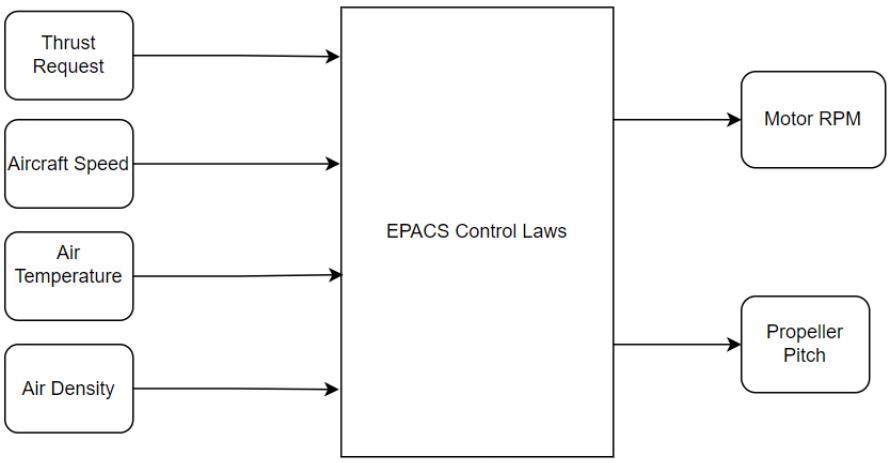

Figure 3.3: EPACS Control Law Basic FlowChart

1. From the inputs received from the Aircraft systems as per the Figure 3.3, the algorithm calculates the mach tip according to (2.1).
2. It is ensured that the mach tip is greater than or equal to 0.5 and less than or equal to 0.8 and if it falls in this desired range. Then an interpolation of the performance maps of C_T is made with respect to the mach number for the motor speed range from 1300 rpm to 1800 rpm with a step size of 50.
3. Once the map specific to the obtained mach number is interpolated, J and C_T are calculated as per (2.2) and (2.3) respectively.
4. With respect to the calculated J value, the second interpolation of C_T maps is done. By this, the different values of C_T that correspond to the obtained J are obtained.
5. The maps are interpolated again for the third time with respect to the newly obtained C_T values to get the corresponding values of C_P.
6. Once C_P is obtained, the η maps are interpolated to obtain the efficiency value corresponding to the C_P and J.
7. The β maps are interpolated to obtain the corresponding blade pitch angle.
8. Once the efficiency values are obtained for the complete speed range, the maximum efficiency value is found out and the RPM and pitch corresponding to this efficiency are given as the output of the function.

3.3 Thermal modelling of the electrical motors

In an effort to develop a comprehensive understanding of the motor's thermal performance, a thermal model was constructed. This model was necessary to account for the change in copper's resistance, a factor significantly influencing the overall copper loss. Furthermore, the effect of a coolant - a water-glycol mixture at a steady temperature of 30 degrees Celsius or 313.15 Kelvin was incorporated into the model. This inclusion allowed to accurately gauge the motor's temperature regulation and

its impact on performance.

The thermal model incorporated a lumped thermal resistance and capacitance value. This was a simplifying assumption that allowed to treat the entire system, from conductor to coolant, as one thermal entity. This approach helped streamline the analysis while still providing a reasonably accurate representation of the system's thermal behavior.

The model was built around five key parameters:

1. **R_{th} - Effective Thermal Resistance of the Machine:** The effective thermal resistance represents the combined resistance of all the individual components in the motor. The lower the thermal resistance, the more efficiently heat can be dissipated from the motor, reducing the risk of overheating and extending the motor's lifespan.

2. **C_{th} - Effective Thermal Capacitance of the Machine:** The effective thermal capacitance takes into account the machine's entire thermal energy storage capacity. A higher thermal capacitance implies that the machine can absorb more heat before its temperature rises, crucial for maintaining performance during periods of high demand.

3. **T_{amb} - Ambient Temperature Surrounding the Machine:** This parameter is the temperature of the environment in which the machine operates, considered a heat sink in our model. The ambient temperature impacts how effectively the machine can dissipate heat into its surroundings, influencing the thermal balance within the system.

4. **$T_{coolant}$ - Coolant Temperature:** The coolant's role is to absorb heat from the machine and transport it away, maintaining a steady operating temperature. The model track the increasing coolant temperature as it flows around the machine, absorbing heat. This factor sets a limit on the motor temperature rise, underscoring the coolant's importance in temperature regulation.

5. **t - Operation Time:** The time, in seconds, during which the machine operates to deliver a particular thrust demand, is another critical factor. This parameter is closely tied to the machine's speed and required input current values, influencing the thermal behavior of the machine over time.

The copper losses of the motors were calculated in this research. To achieve this, an updated loss model integrated with a thermal model was employed, which is represented graphically in Figure 3.4.

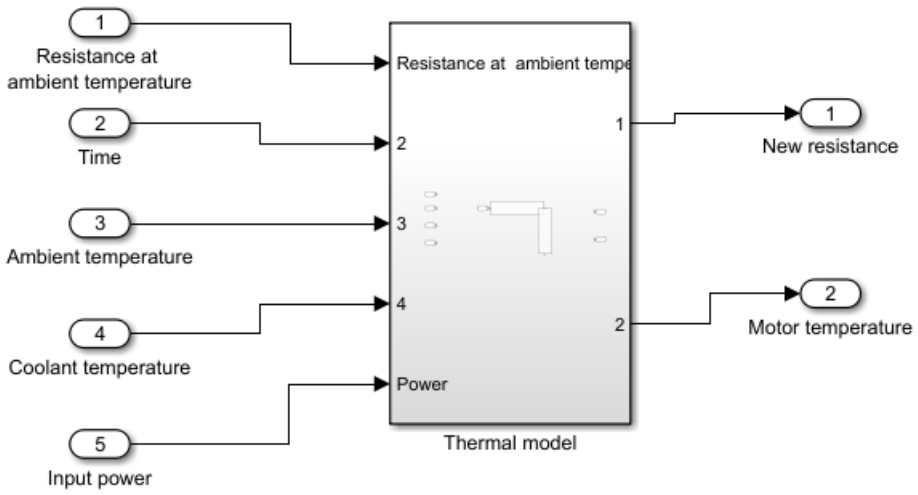

Figure 3.4: Thermal model subsystem

The thermal model served as a blueprint for the system, outlining the fundamental aspects of the calculations. The following systematic process was followed to construct and implement this model:

1. Defining several key parameters, including thermal resistance and capacitance, operational time, power, coolant temperature, and ambient temperature. These values were drawn from a performance sheet and tested to identify the optimal test points.

2. Incorporating the coolant temperature into the model. The coolant's role in maintaining optimal temperature range within the motor is vital, and its temperature increase concerning operational time as well as the maximum achieved temperature it can get to in one working cycle had to be accounted for. The architecture ensures that the coolant is also cooled to provide a lower ambient temperature to the motors.

3. Once the coolant's temperature had been included, the motor temperature was updated, employing the lumped parameter network model for this purpose. Given that power input is critical to understanding a motor's thermal behavior, it was assumed to be constant for each case in this step, aiding in maintaining consistency across the calculations.

4. Finally, with the updated motor temperature, the final resistance value was revised. This step is crucial as the resistance directly impacts the motor's performance, and any changes in temperature can significantly alter this parameter.

To calculate the winding temperature, the dynamic thermal model from Chapter 2.4.4 is discretized. For each time step, the winding temperature is calculated and updated, and the winding resistance is updated together with the copper losses. The same algorithm is then looped until the operation time is completed or the steady state has been achieved, with the looped interval equal to the chosen time step. The coolant temperature is increased until a steady value of 40°C has been achieved. The equations used in the algorithm are,

$$T_{coolant} = min(T_{coolant} + 10/60 * Ts, 40) \tag{3.1}$$

$$T_{winding} = T_{coolant} + (T_{winding,prev} - T_{coolant}) * e^{-Ts/(R_{th} * C_{th})} + P_{Cu,loss} * Ts/C_{th} \tag{3.2}$$

$$R_s = R_{s,at20C} * (1 + 0.00393 * (T_{winding} - T_{winding,at20C})) \tag{3.3}$$

where $T_{coolant}$ is the coolant temperature, $T_{winding}$ is the motor temperature, $T_{winding,prev}$ is the last updated motor temperature that is obtained from the loop, Ts is the sample time step within the loop, R_{th} is the thermal resistance, C_{th} is the thermal capacitance, $P_{Cu,loss}$ is the copper loss, $R_{s,at20C}$ is the motor resistance at base temperature, $T_{winding,at20C}$ is the motor winding base temperature, and R_s is the updated motor resistance at higher temperatures. The constant 0.00393 refers to the copper's resistance temperature coefficient calculated at the base temperature.

The resistance value derived from this process, for each winding, was then utilized in calculating the motor losses. It was scaled to encompass the three parallel winding in the four motors working in tandem inside the electrical unit in the ES-30 aircraft as,

$$I = \sqrt{i_d^2 + i_q^2} \tag{3.4}$$

$$P_{Cu,loss} = (I^2) * (R_s/3) * 4 \tag{3.5}$$

where I is the motor current obtained from the dq model, i_d and i_q are the motor currents in the d and q axes respectively, R_s is the updated motor resistance from the thermal model and $P_{Cu,loss}$ is the copper loss for the entire electrical propulsion unit. The copper losses are updated in the loop, with final values depending on the duration of the operation.

3.4 Building the electrical propulsion system model for updated propulsion performance optimisation

The same algorithm, used for propeller performance optimisation, was employed for motor efficiency calculations. These calculations included motor losses as a function of current, a variable integral to calculating the motor's efficiency and the overall

Electric Propulsion Unit's (EPU - a system encompassing the motor and inverter) efficiency. Utilizing this methodology, the highest efficiency values were determined and the optimal pitch angles corresponding to these efficiencies were identified by navigating through the performance maps.

Due to the varying nature of the parameters of the calculations, the propeller and motor values didn't always align perfectly with the fixed data points in the performance maps. Therefore, the propeller maps were interpolated to bridge the gap between our calculated values and the existing data points. This enabled to maintain the accuracy and reliability of the results while adapting to the unique challenges presented by the study.

Once these results were achieved, a comparative analysis was initiated, aligning these findings with the results obtained from the propeller performance algorithm. This comparison was primarily based on speed and pitch angle parameters since the highest efficiency value effectively determined the final operation points. Interestingly, the two models revealed distinct degrees of influence over the optimal point determination process.

While both the propeller performance model and the EPU efficiency model contributed to identifying the operation points, they did so at varying intensities. The model with higher losses exerted a more substantial influence on efficiency, and as such, the final operating point gravitated more towards its determined values. In essence, the weight of influence shifted more towards the model indicating higher losses, leading to the identified optimal points leaning more towards its values.

It's important to reiterate that these findings do not represent an anomaly or a flaw in the algorithm. Rather, they reveal the inherent intricacies of the system's efficiency dynamics and emphasize the need for an adaptive approach towards optimization. Therefore, this study contributes not only to enhancing our understanding of electric propulsion system optimization but also to the broader discourse on efficient and sustainable aviation.

4

Results and Discussions

The performance of the propulsion system was optimised and analysed for the Take Off, Climb and Cruise phases as mentioned in Chapter 2.1.1. Table 4.1 describes these phases with their characteristics at normalized thrust values. Further the most common values for air density and the aircraft speed, stemming from exhaustive aircraft performance simulations, were used during all flight phases. Especially in the cases of Take-Off and Climb, where these values are constantly changing, using the typical values, with more weight given to the ones found at the worst case scenario, led to an easier understanding and clear analysis of the effects of other varying parameters.

Table 4.1: Characteristics of the Flight Phases with Normalized Thrust Values

Phases	**Thrust Demand (%)**	**Aircraft Speed(m/s)**	**Air Density (kg/m^3)**
Take Off	100	52	1.225
Climb	59	90	0.9046
Cruise at 10k ft	30	89.5	0.9046
Cruise at 20k ft	29	104.9	0.6526
Cruise at 20k ft at Max Speed	35	132	0.6526

4.1 Propeller Performance

The optimum efficiency and hence the RPM - pitch combinations for the propeller were found out for each of the 5 phases by performing the algorithm described in Chapter 3.2. The relationship of torque and efficiency with speed was plotted.
Figure 4.1 represents the behaviour of the propeller during Take Off. It was observed that the highest efficiency is always obtained at the highest motor rpm, which is 1750 in this case. Further analysis led to the inference that the Climb phase and Cruise at maximum speed phase also exhibit the same behaviour as seen in the take off phase. The similarity that can be drawn between these three phases is that they have relatively higher thrust demands when compared to the other phases.
Similarly, Figure 4.2 represents the behaviour of the propeller during Cruise at 10k ft altitude. Unlike the Take off phase, here the best efficiency is achieved at the lowest motor rpm i.e., 1300. This exact behaviour can also be observed in the case of the Cruise phase at 20k ft altitude. Thus, it can be stated that this behaviour

can be attributed to phases with lower thrust demands.

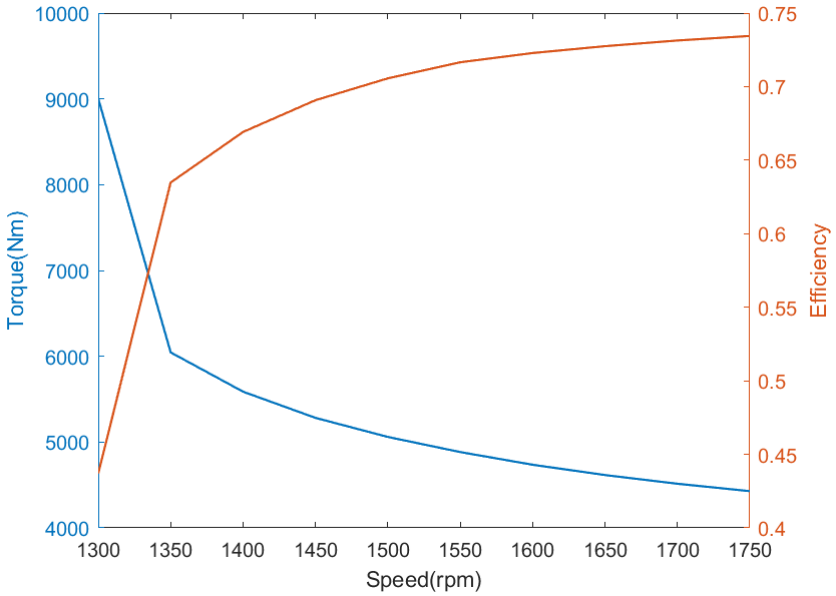

Figure 4.1: Torque Vs Speed Vs Efficiency Graph of Propeller for Take Off

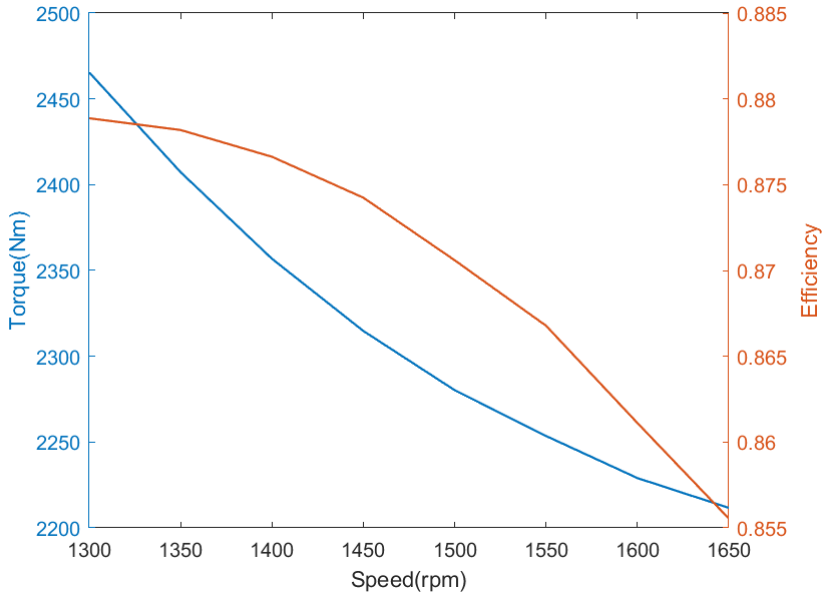

Figure 4.2: Torque Vs Speed Vs Efficiency Graph of Propeller for Cruise

4.2 Loss models for electric propulsion unit

The following graphs have been obtained for the motor loss models, the inverters and the updated graphs for the propellers. This was done to provide a comparison in the working of the propellers, with respect to their original operational points

determined by the speed and the efficiency. The graphs give insight on the motor workings and the way the propulsion system and the thermal losses affect the operating points.

The first step in validating the developed thermal model was to analyse the behaviour of the motor losses with torque and speed. Figure 4.3 represents the motor losses plotted as a function of torque and speed during take off. It can be observed that the motor losses increase with torque, thus being consistent with the expected behaviour of the losses of a PMSM machine. Similar graphs were obtained for the other phases as well.

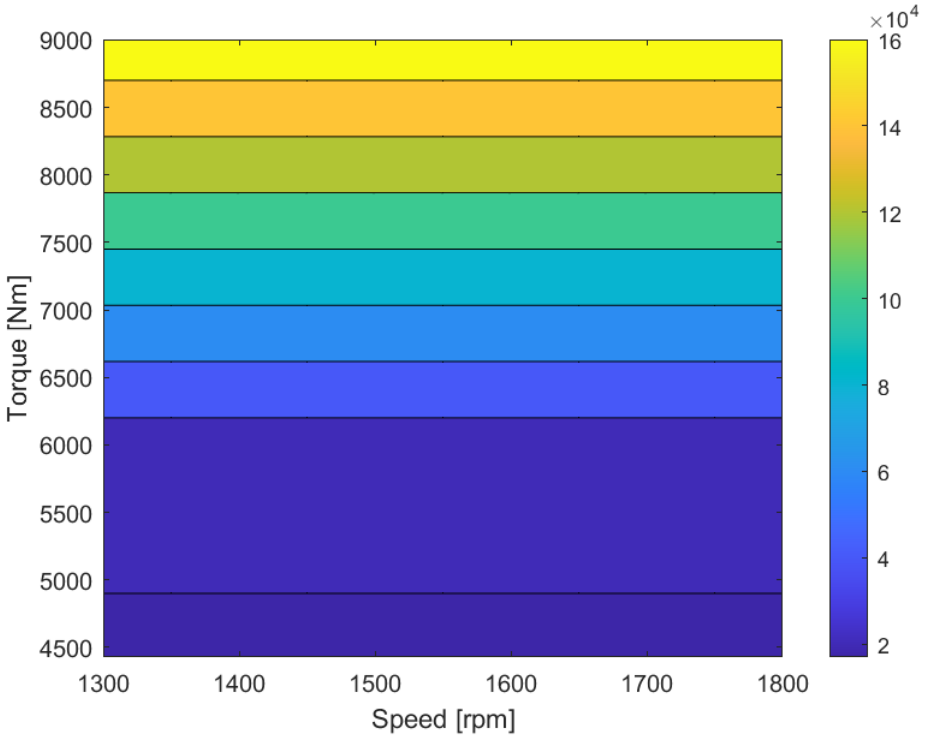

Figure 4.3: Motor Loss Map for Take Off

Figure 4.4 displays the relationship between motor temperature and the operating time. Due to the presence of the coolant, the temperature curve is a parabolic function which reaches a stable value eventually. This depends on the coolant time constant, which was close to 250 seconds, and thus the time to reach a steady state was found to be approximately 1250 seconds of continuous operation.
To confirm the validity of the model, it was cross-verified with the motor performance sheet. This step helped to ensure that the findings were in line with the motor's documented performance and within the acceptable operational limits and conditions. In essence, through this methodical process, a robust and reliable thermal model was developed that captures the nuanced aspects of motor operation. It not only offers insights into the motor's thermal behavior but also provides a framework for understanding and minimizing motor losses, ultimately contributing to the development of more efficient electric aircraft propulsion systems.

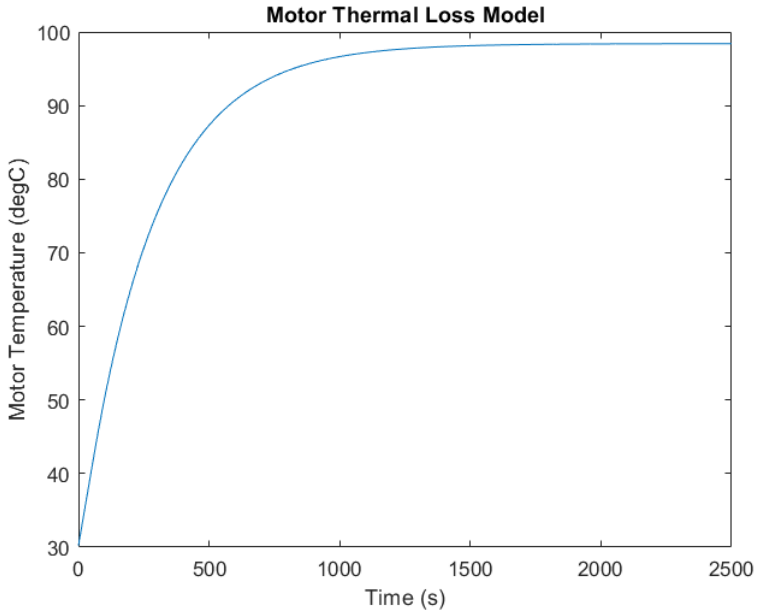

Figure 4.4: Motor temperature in relation to time

The main motive behind developing a thermal model for the motor was to calculate the losses that change dynamically with the temperature. Building upon the updated temperature values derived from the motor thermal model, the winding resistance for the unit was updated. In Figure 4.5 the relation between the winding resistance of the unit and the motor temperature is shown.

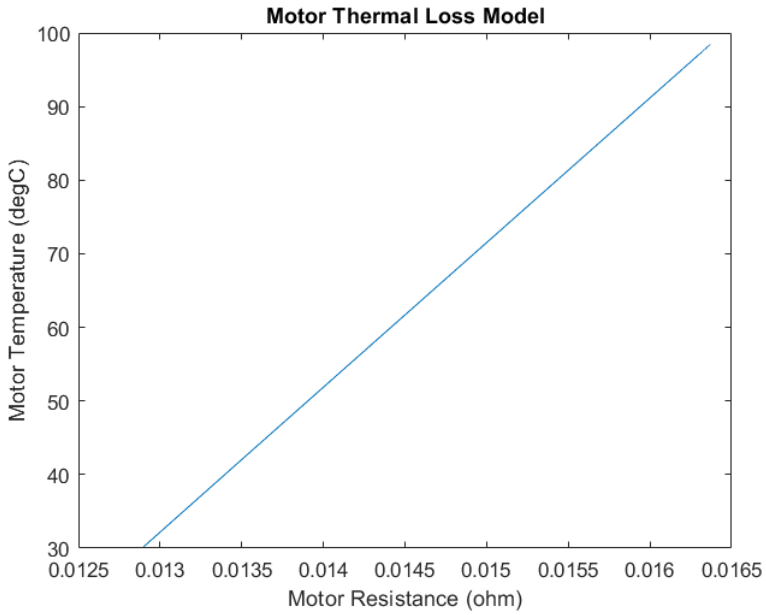

Figure 4.5: Motor winding resistance vs temperature

The copper losses of the motor occur due to the resistance in the motor winding. When the motor torque increases, the motor current increases, resulting in an increase in the voltage drop across the winding, which in turn results in the increase

of the motor copper losses. Therefore, the copper losses are effectively quadratically proportional to the motor torque. This is represented in Figure 4.6. The parameters are plotted in per unit to account for the general behaviour across all the flight profiles.

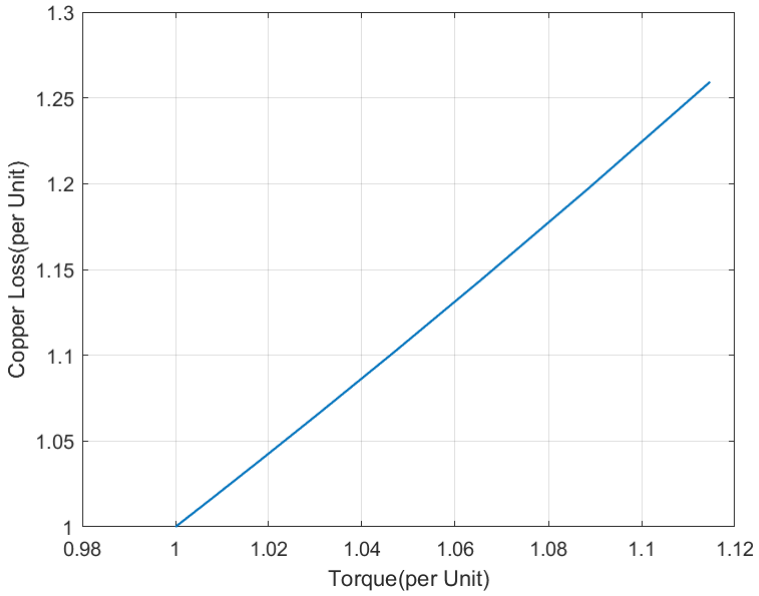

Figure 4.6: Copper loss relation with Motor Torque

Figure 4.7 reflects the more linear relationship the copper losses have with the motor resistance and ultimately the motor temperature. As mentioned, the losses increase until the thermal steady state has been achieved by the electrical motor, after which they remain constant for the remaining duration of the operation.

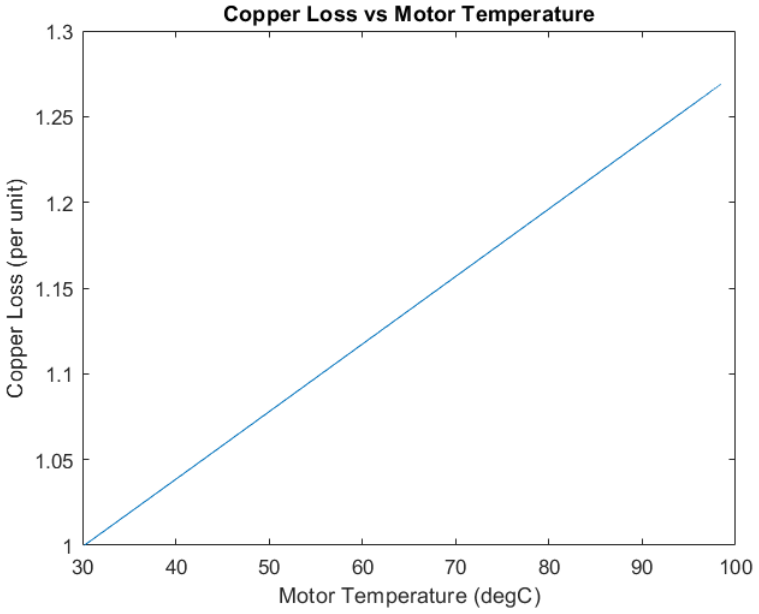

Figure 4.7: Copper loss relation with motor temperature

The core losses for the motor were also interpolated from the performance sheet provided by the supplier. It was found that these losses are very linear with speed and therefore they were plotted as a function of motor speed which is the output variable of the thrust controlled propulsion function. An important thing to note here is that the interpolated losses was found to be independent of motor torque, and thus follow the same relation for all the considered flight profiles.

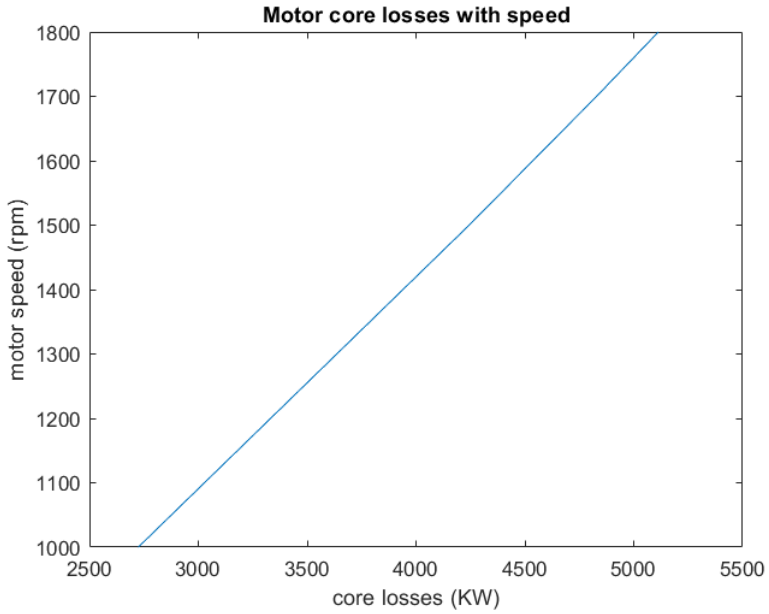

Figure 4.8: Core loss relation with motor speed

Figure 4.9 corresponds to the inverter losses, plotted for one device as a function of electric current. Since there are four inverters, the losses need to be further multiplied to contribute to the final loss model. These conduction losses are given for a fixed input voltage and switching frequency values, and have been assumed to follow the same relationship with current for all flight profiles. The losses were taken from the values provided by the supplier, and they have been further interpolated to account for the finer values of current, not captured in the data sheet provided by the supplier.

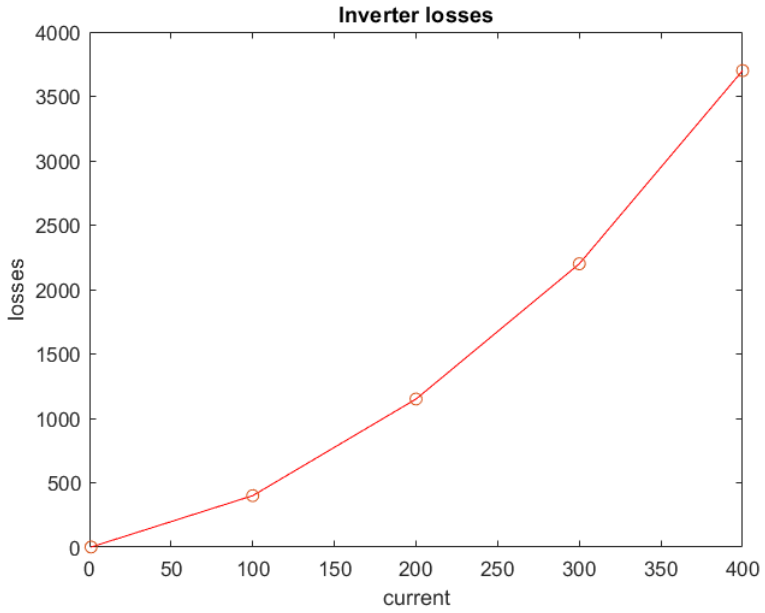

Figure 4.9: Single inverter loss with motor current

4.3 Comparison of Results

In this section, the objective is to paint a contrast between the propeller performance under two distinct scenarios. First, the scenario where only the propeller-specific parameters are factored into the equation is examined. Following this, the impact of integrating the Electrical Propulsion Unit (EPU) model into the propeller model is investigated. These evaluations are conducted separately for each phase of flight, and a direct comparison is carried out in every instance, facilitating a deeper understanding of the dynamics at play.
Upon evaluating the results, a notable resemblance was evident from the trends observed across different phases. Based on the results, the phases are classified into two categories : Phases with higher thrust demand and Phases with lower thrust demand.

4.3.1 Phases with higher thrust demand

This category includes the Take Off, Climb and Cruise at 20k ft altitude at maximum speed. As mentioned in Chapter 2.2, the Take Off is the flight phase which has the highest thrust demand. From Figure 4.10, it can be observed that the optimised operating point for propeller, motor and the whole system is exactly the same at the highest motor rpm and the optimum points are summarized in Table 4.2. The motor losses are highest during the take off phase owing to the comparatively low motor efficiency, stemming from the non-overlapping areas of the optimal operation of motor and propellers, based on their respective torque and speed here. The same trend can be observed from the results of the other two phases and therefore only the optimum points are shown in Tables 4.3 and 4.4.

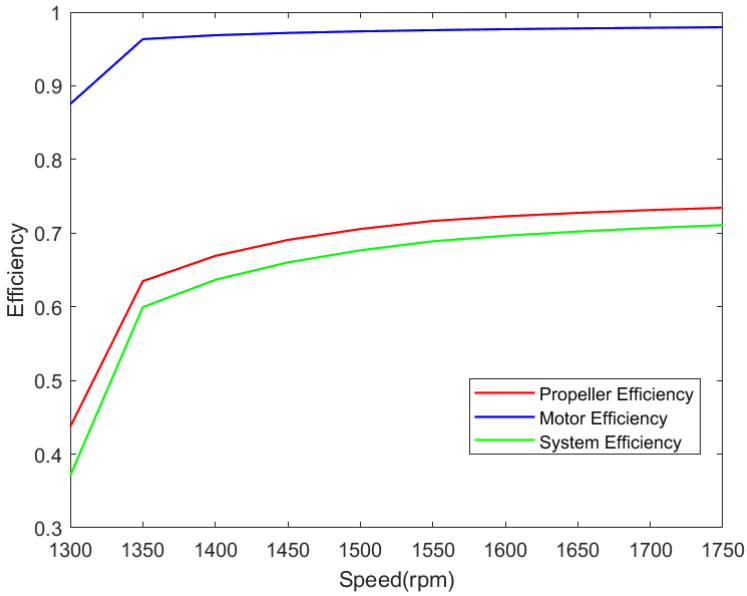

Figure 4.10: Efficiency comparison for Take Off

Table 4.2: Take Off Results

Parameters	Propeller	Motor	System
Maximum ETA	0.7344	0.948	0.688
RPM	1750	1750	1750
Pitch	20.389	20.389	20.389

Table 4.3: Climb Results

Parameters	Propeller	Motor	System
Maximum ETA	0.8485	0.9548	0.8009
RPM	1650	1650	1650
Pitch	29.15	29.15	29.15

Table 4.4: Cruise at Max Speed Results

Parameters	Propeller	Motor	System
Maximum ETA	0.8845	0.9615	0.8411
RPM	1550	1550	1550
Pitch	38.60	38.60	38.60

4.3.2 Phases with Lower Thrust Demand

The two cruise phases, i.e., Cruise at 10k ft altitude and Cruise at 20k ft altitude are included in this category. Here, different optimised operating points were obtained

for each of the component. While the highest efficiency for propeller was obtained at lowest motor rpm, that of motor was obtained at a higher motor rpm as can be seen in Figure 4.11. Consequently, the optimised operating point for the whole system was found out to be a balanced combination of the two components. In Table 4.5 the different optimum points are shown for Cruise at 10k ft and in Table 4.6 the results for Cruise at 20k ft are shown.

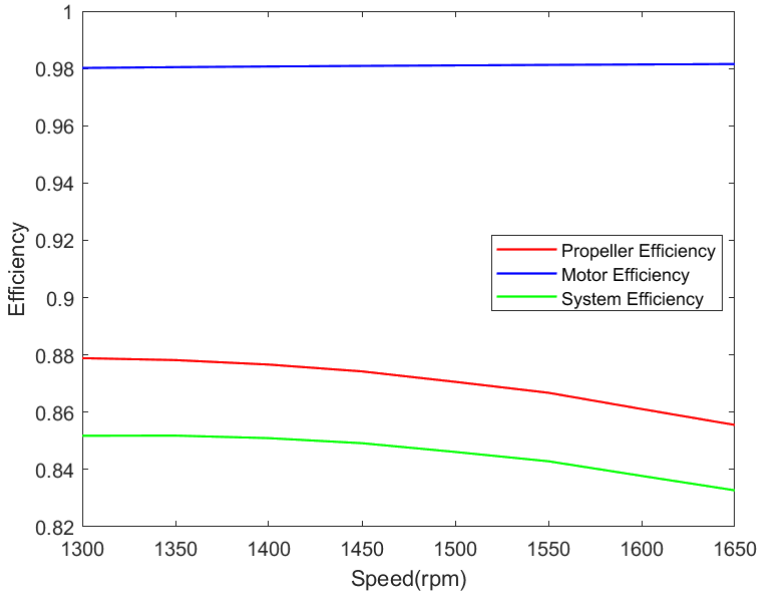

Figure 4.11: Efficiency Comparison for Cruise at 10k ft

Table 4.5: Cruise at 10k ft Results

Parameters	Propeller	Motor	System
Maximum ETA	0.8788	0.9726	0.8414
RPM	1300	1650	1350
Pitch	33.029	25.27	31.69

Table 4.6: Cruise at 20k ft Results

Parameters	Propeller	Motor	System
Maximum ETA	0.8785	0.9722	0.8447
RPM	1450	1650	1550
Pitch	34.624	30.03	32.22

4.4 Discussion

As a final evaluation, the average efficiencies of the propeller model and system model were calculated across the Take Off, Climb and Cruise Phases. The duration

was estimated to be 1 minute, 15 minutes and 30 minutes for take-off, climb and cruise respectively. In Tables 4.7 and 4.8 the average system efficiency is calculated for when the propeller speed and pitch is selected to only optimize the propeller efficiency and when they instead are selected to optimize the system efficiency. Since the Cruise part is the longest part of the flight the average system efficiency becomes slightly higher if the optimization is done to maximize the system efficiency. A higher average efficiency means that less energy is used for the flight.

Table 4.7: Average system efficiency when only optimizing for the highest propeller efficiency

Flight mode	**Time**	**Optimized for max propeller efficiency**		
		Propeller	**Motor**	**System**
Take Off	1 min	73.44%	94.8%	68.8%
Climb	15 min	84.85%	95.48%	80.09%
Cruise 10k ft	30 min	87.88%	96.71%	84.06%
	Average			82.43%

Table 4.8: Average system efficiency when the system efficiency is maximized

Flight mode	**Time**	**Optimized for max system efficiency**		
		Propeller	**Motor**	**System**
Take Off	1 min	73.44%	94.8%	68.8%
Climb	15 min	84.85%	95.48%	80.09%
Cruise 10k ft	30 min	87.81%	96.88%	84.14%
	Average			82.49%

Building on the foundational insights generated from this study, we believe that the potential for electric aviation is immense and yet to be fully realized. The exploration of the complex interplay between the propeller and EPU has opened up avenues for targeted enhancements that can further increase system efficiency. This efficiency drive is paramount in a world increasingly concerned with sustainability and the reduction of carbon emissions. It places electric aviation at the forefront of these global efforts, offering a promising alternative to traditional combustion-engine aircraft.

Interestingly, our study revealed the relationship between the presumed role of the propeller placed in parallel with the electrical components in determining system efficiency. It showcased the significance of propeller design and operation, challenging the commonly held notion that motors and power electronics are the sole drivers of efficiency. This shift in understanding can have substantial implications for future research and development in the field, redirecting focus towards more efficient propeller designs and operation strategies.

The implications of our findings extend beyond just the observed components of the electric propulsion system. They also hint at the potential for more radical

architectural changes within the system. Thinking about future alterations in the system architecture, we considered several potential adaptations. This included introducing redundant electrical support, considering alternative motor connections, and rethinking power electronic and battery connections, either to the entire motor as a whole or to each winding individually. Such system modifications hold the potential to enhance system robustness and optimize performance.

While we are already witnessing the dawn of the electric aviation era, the full potential of this technology is yet to be explored. Electric aircraft hold the promise of a cleaner, more sustainable future for aviation. As such, this thesis serves as an important piece of a much larger puzzle.

In essence, this study contributes to the ongoing discourse on electric aviation, providing empirical evidence that highlights the critical role of propellers and EPUs in determining system efficiency. It serves as a stepping stone, encouraging further exploration of architectural improvements and shedding light on potential areas of optimization. As we move forward, we are excited about the potential of these findings to drive innovation and contribute to the broader endeavor of making electric aviation a viable and sustainable reality.

5

Conclusion

This study undertook a comprehensive analysis with a focus on the dual aspects of an electric aircraft propulsion system: the propeller and the Electric Power Unit (EPU). Their individual contributions as well as their combined influence on the system's performance were investigated. This detailed examination has unearthed intriguing insights, revealing not only the unique characteristics of each component but also their intricate interplay within different flight phases.

The initial hypothesis of the work centred on the idea that the propeller, being the higher loss-making element, would significantly influence efficiency determination. In contrast, it was expected that the electrical motors and power electronic devices, given their higher inherent efficiency, to have a less substantial impact on overall system efficiency.

To validate this hypothesis a propeller model was compared with an EPU loss model, utilizing the performance parameters provided by the propeller supplier. A thermal loss model was introduced for the motors to account for losses due to resistance increase over time together with loss models for motor core losses and inverter losses. The simulation results corroborated the initial hypothesis, demonstrating a strong alignment and thus reinforcing the understanding of the performance dynamics in electric propulsion systems. To optimize the system efficiency the RPM - pitch combinations for the Take off, Climb and Cruise flight phases were determined to be 1750 rpm and 20.3°, 1650 rpm and 29.15°, 1350 rpm and 31.7°respectively. Finally, the average efficiency result calculations also reiterated the importance of integrating the EPU loss model with the propeller loss model and the average system efficiency increased from 82.43 % to 82.49 % when optimizing for system efficiency compared to only propeller efficiency.

In conclusion, this study underscores the importance of a detailed understanding of each component's role in an electric propulsion system. Further, it highlights the potential for efficiency optimization through system-level improvements and sets the stage for future research in this exciting field.

5.1 Future scope of the study

Considering the vital role of propellers in system efficiency, we foresee a surge in research and development centered on propeller design and operational efficiency. Future innovations could encompass smarter, variable pitch propellers that adapt real-time to varying flight conditions, optimizing thrust while minimizing energy consumption. These strategies could push the boundaries of what is currently achievable, enhancing system robustness, reliability, and performance.

Similarly, the electric power unit (EPU), a key component of the electric propulsion system, presents its own set of innovation opportunities. Advancements in materials science and engineering could lead to the development of lighter, more energy-efficient EPUs, enhancing flight endurance and overall efficiency. Future research might also explore the possibility of adaptive EPUs, capable of altering their performance characteristics in response to different flight phases.

Additionally, our study pointed towards the potential benefits of more radical system architecture changes. The integration of AI and machine learning algorithms into the system could very well change a lot of things. These algorithms can continuously analyze flight data, making real-time adjustments to the propulsion system components for optimal efficiency. Concepts such as battery swapping or ultra-fast charging technologies, going hand in hand with research and experimentation to build more energy dense batteries, could also be worth investigating as possible solutions to the present limitations in energy storage technology.

It is hoped that future innovators will take the baton from here, using the insights and questions raised in this study as a springboard to drive the next wave of breakthroughs in the field of electric aviation.

5.2 Ethical considerations and responsible research practices

Throughout the course of our research and thesis development on the electrical propulsion system of the ES-30 electric aircraft, we have held responsible research practices and ethical considerations at the forefront of our work. These principles have not only informed our scientific approach but also shaped our relationships with our colleagues, advisors, and the wider academic community.

From the outset, we recognized the need for full transparency and accuracy in our research. This was necessary not only for the integrity of our work but also to ensure that our findings could be effectively utilized by others in the field. The nature of our study also required us to engage with a broad range of proprietary and sensitive data, especially concerning the proprietary technology of Heart Aerospace AB's ES-30 electric aircraft. We deeply respect the confidentiality and intellectual

property rights associated with this information. As such, we always ensured proper authorization was granted before accessing or utilizing any of this data. We also committed to the appropriate citation and acknowledgement of all sources and contributions to our research, aiming to uphold academic integrity and avoid any form of plagiarism.

We maintained open lines of communication with our advisors and colleagues at all times. We embraced a spirit of cooperation and mutual respect, believing that collaboration is essential to advancing knowledge and innovation. Feedback and constructive criticism were actively sought and considered in our research processes.

Furthermore, we were conscious of the potential societal and environmental implications of our work. As we researched the ES-30's electrical propulsion system, we were aware of our responsibility to consider the environmental sustainability of our findings. Our goal was to contribute to a future of aviation that is not only technologically advanced but also environmentally responsible. As engineers, we also understood the safety considerations associated with aircraft design and operation. We never lost sight of the fact that our work could potentially impact the lives of real people, and we carried that responsibility with utmost seriousness.

Lastly, we believe that the fruits of research should be shared with the community. Hence, we committed to publishing our findings in an accessible and comprehensible manner, which could be beneficial to other researchers, engineers, and the public at large.

In summary, our research was guided by a strong ethical compass and a deep commitment to responsible research practices. We are proud of the work we have accomplished and believe that upholding these principles has not only enhanced the quality of our thesis but also fostered a better understanding of the critical importance of ethics and responsibility in scientific research.

References

[1] Budd, L., Griggs, S., 'I&' Howarth, D. (Eds.). (2013). Sustainable aviation futures. Emerald Publishing Limited.

[2] Epstein, A. H., O'Flarity, S. M. (2019). Considerations for Reducing Aviation's CO2 with Aircraft Electric Propulsion. Journal of Propulsion and Power, 35(3), 572–582. doi:10.2514/1.B37015

[3] P. Wheeler, T. S. Sirimanna, S. Bozhko and K. S. Haran, "Electric/Hybrid-Electric Aircraft Propulsion Systems," in Proceedings of the IEEE, vol. 109, no. 6, pp. 1115-1127, June 2021, doi: 10.1109/JPROC.2021.3073291.

[4] Jansen, R., Bowman, C., Jankovsky, A., Dyson, R., Felder, J. (2017). Overview of NASA Electrified Aircraft Propulsion (EAP) Research for Large Subsonic Transports. 53rd AIAA/SAE/ASEE Joint Propulsion Conference. doi:10.2514/6.2017-4701

[5] Brelje, B. J., Martins, J. R. R. A. (2018). Electric, hybrid, and turboelectric fixed-wing aircraft: A review of concepts, models, and design approaches. Progress in Aerospace Sciences. doi:10.1016/j.paerosci.2018.06.00

[6] Talay, Theodore A. Introduction to the Aerodynamics of Flight. NASA., 1975.

[7] Pilot's Handbook of Aeronautical Knowledge. (2016). U.S. Department of Transportation, Federal Aviation Administration, Flight Standards Service.

[8] Airplane Flying Handbook: FAA-H-8083-3C (2022). New York, NY: Skyhorse Publishing.

[9] Bright Appiah Adu-Gyamfi, Clara Good, Electric aviation: A review of concepts and enabling technologies, lTransportation Engineering, Volume 9,2022,100134,ISSN 2666-691X, https://doi.org/10.1016/j.treng.2022.100134. (https://www.sciencedirect.com/science/article/pii/S2666691X2200032X)

[10] Gesell, H., Wolters, F., Plohr, M. (2019). System analysis of turbo-electric and hybrid-electric propulsion systems on a regional aircraft. The Aeronautical Journal, 123(1268), 1602-1617. doi:10.1017/aer.2019.61

[11] Zhang J, Roumeliotis I, Zolotas A. Sustainable Aviation Electrification: A Comprehensive Review of Electric Propulsion System Architectures, Energy Management, and Control. Sustainability. 2022; 14(10):5880. https://doi.org/10.3390/su14105880

[12] Rendón, M.A., Sánchez R., C.D., Gallo M., J. et al. Aircraft Hybrid-Electric Propulsion: Development Trends, Challenges and Opportunities. J Control Autom Electr Syst 32, 1244–1268 (2021). https://doi.org/10.1007/s40313-021-00740-x

[13] A. Loganayaki and R. B. Kumar, "Permanent Magnet Synchronous Motor for Electric Vehicle Applications," 2019 5th International Conference on Advanced

Computing Ì&’ Communication Systems (ICACCS), Coimbatore, India, 2019, pp. 1064-1069, doi: 10.1109/ICACCS.2019.8728442.

[14] Y. Xu, Q. Li, L. Zhang and Q. Ma, "Development of permanent magnet synchronous motor for electric vehicle," 2009 International Conference on Sustainable Power Generation and Supply, Nanjing, China, 2009, pp. 1-5, doi: 10.1109/SUPERGEN.2009.5348015.

[15] Caicedo Parra, D., Ramakrishnan, K., Farrell, L., Narula, M. et al., "A Lumped-Parameter Thermal Model for System Level Simulations of Hybrid Vehicles," SAE Technical Paper 2020-01-0150, 2020, https://doi.org/10.4271/2020-01-0150.

[16] Gudmundsson, S. (2014) General Aviation Aircraft Design: Applied Methods and procedures. Amsterdam: Butterworth-Heineman is an imprint of Elsevier.

[17] Hitchens, F. (2015), Propeller aerodynamics : The history, aerodynamics Ì&’ operation of aircraft propellers. Andrews UK Ltd..

[18] Jianhua Xu et al 2019 IOP Conf. Ser.: Mater. Sci. Eng. 686 012019, DOI 10.1088/1757-899X/686/1/012019

[19] Jenkins, F. A., White, H. D., ‘I&’ Delsanto, P. P. (2015). Fundamentals of Optics (4th ed.). McGraw-Hill Education

[20] Demetriades, G. D., et al. (2019). Design, Implementation and Characterization of a High-Speed Surface Permanent Magnet Motor with Minimum Air Gap. Energies, 12(13), 2529

[21] Smith, J., ‘I&’ Rife, M. (2018). Electric Motors and Drives: Fundamentals, Types and Applications (4th ed.). Elsevier

[22] Han, Z., Wu, B., Liu, Z., ‘I&’ Xu, D. (2019). Design and analysis of electric aircraft propulsion systems. IEEE Access, 7, 102699-102714

[23] Rastogi, A., Liang, J., Yilmaz, M., ‘I&’ Gligor, A. (2017). Design and analysis of electrical power system architectures for distributed electric propulsion aircraft

[24] Hu, X., Xu, L., ‘I&’ Liu, L. (2019). A review on battery management system of electric vehicles: Challenges and opportunities. Energy Procedia, 158, 3999-4006

[25] Vaez-Zadeh, Sadegh, Control of Permanent Magnet Synchronous Motors (Oxford, 2018; online edn, Oxford Academic, 19 Apr. 2018), https://doi.org/10.1093/oso/9780198742968.001.0001, accessed 19 July 2023.

A

Appendix 1

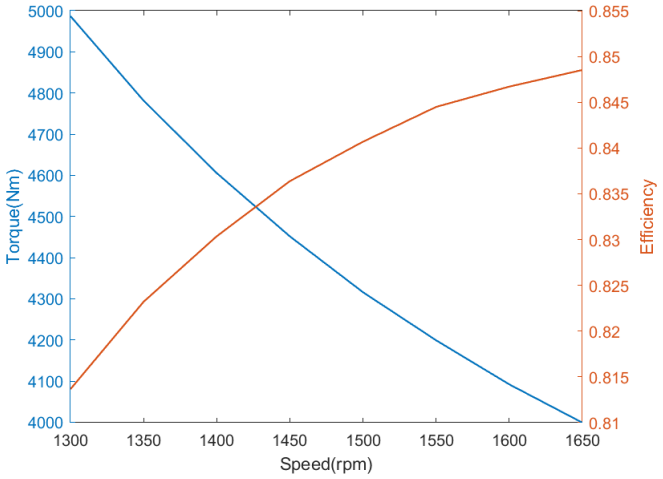

Figure A.1: Torque Vs Speed Vs Efficiency Graph of Propeller of Climb

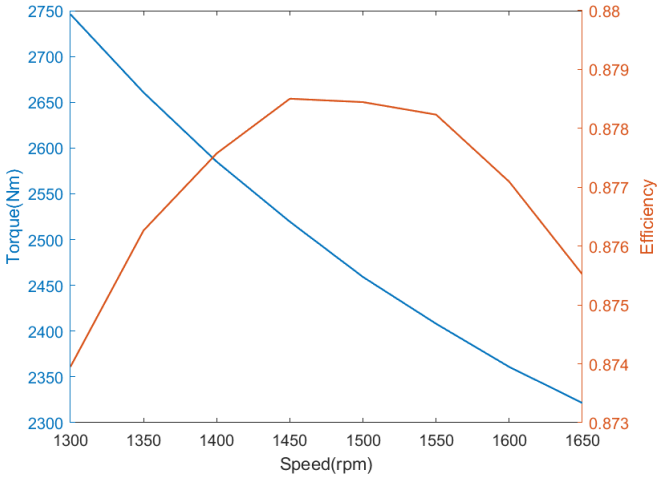

Figure A.2: Torque Vs Speed Vs Efficiency Graph of Propeller for Cruise at 20k ft

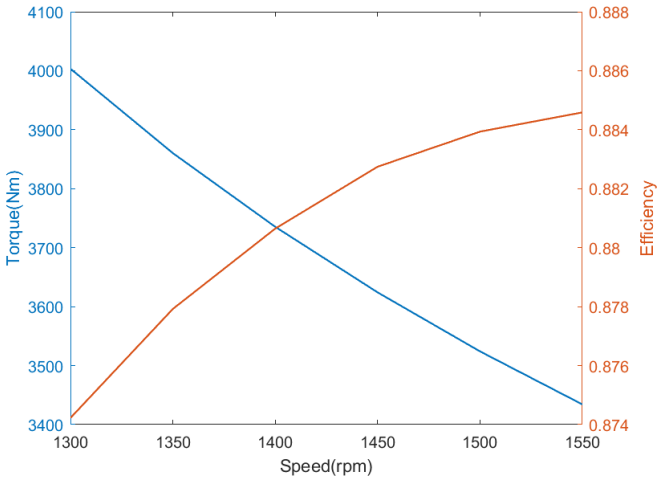

Figure A.3: Torque Vs Speed Vs Efficiency Graph of Propeller for Cruise at Max Speed

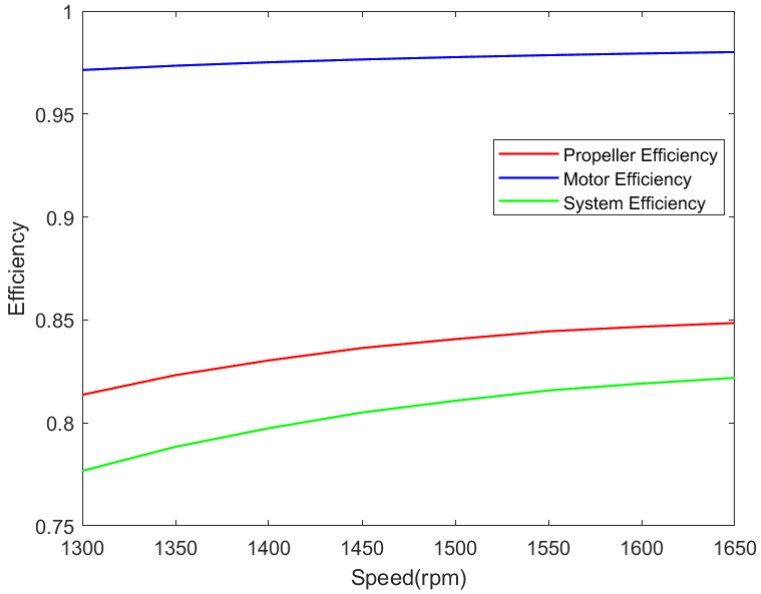

Figure A.4: Efficiency Comparison during Climb

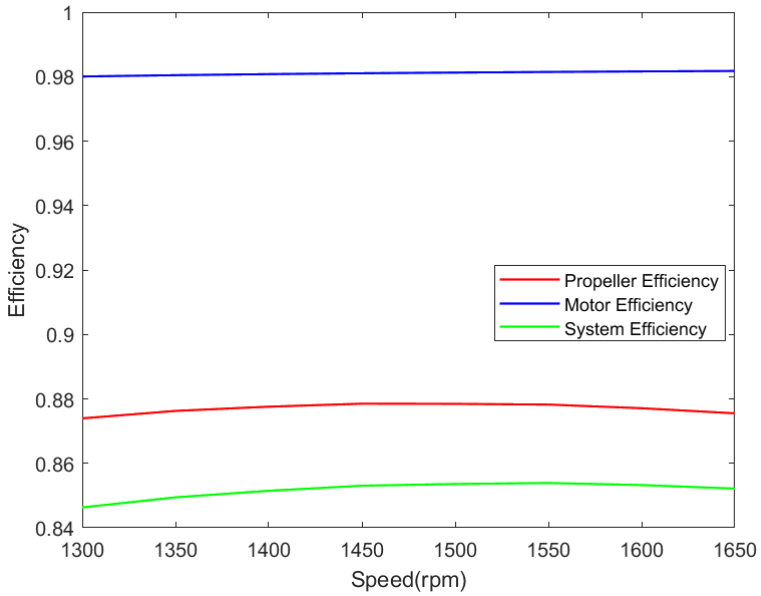

Figure A.5: Efficiency Comparisom during Cruise at 20k ft

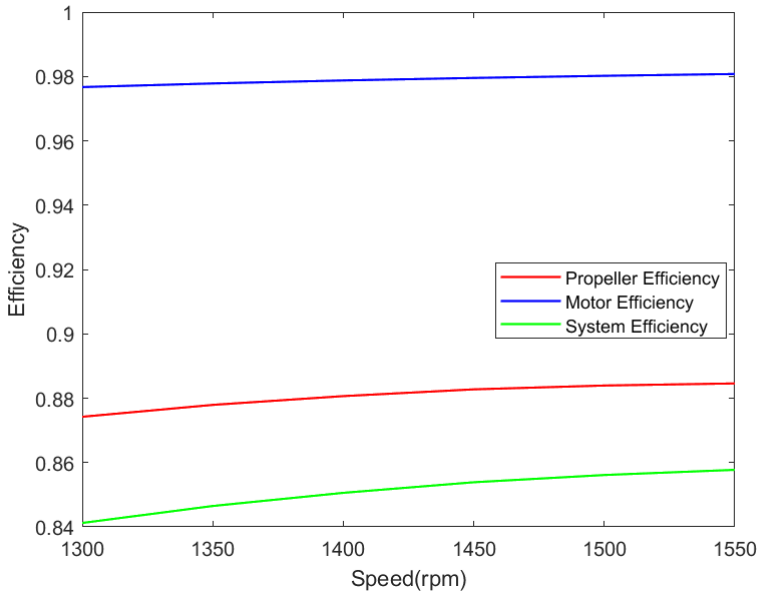

Figure A.6: Efficiency Comparison during Cruise at Max Speed

DEPARTMENT OF SOME SUBJECT OR TECHNOLOGY
CHALMERS UNIVERSITY OF TECHNOLOGY
Gothenburg, Sweden
www.chalmers.se

CHALMERS
UNIVERSITY OF TECHNOLOGY